

Electron properties of carbon nanotubes in a periodic potential

Dmitry S. Novikov*

Department of Electrical Engineering and Department of Physics, Princeton University, Princeton, NJ 08544 and
Department of Physics, Massachusetts Institute of Technology, Cambridge, MA 02139

(Dated: May 23, 2019)

Coupling of nanotube electrons to an external periodic potential is suggested as a means to demonstrate and study effects of strong electron interactions, including Wigner crystallization, commensurate–incommensurate transitions, Tomonaga–Luttinger correlations, and spin excitations of high symmetry. Electron interactions result in a devil’s staircase of incompressible states that correspond to the electron density (counted from half-filling) commensurate with the potential period. The Dirac nature of the nanotube’s four fermion modes with an approximate $SU(4)$ symmetry allows for a non-perturbative bosonized treatment of both electron–electron interactions and coupling to the external potential. Excitation gaps for the incompressible states are estimated using the phase soliton approach that describes a slow deformation of the regular quantum soliton lattice representing nanotube electrons locked by the external potential.

In the limit when electron wave functions are delocalized, incompressible electron states and excitation gaps are described in terms of the narrow gap Luttinger liquid of the four flavors. Charge gaps are heavily renormalized due to quantum fluctuations of the neutral sector, whereas neutral excitations are governed by the effective $SU(4) \simeq O(6)$ Gross–Neveu Lagrangian. In the opposite limit of the localized electrons, effects of exchange are unimportant, and the electron system behaves as a single fermion mode that represents a Wigner crystal locked by the external potential. The phase diagram is drawn using the effective single mode Hamiltonian derived for strongly interacting nanotube electrons in this limit.

Incompressible states can be detected by utilizing the adiabatic transport setup proposed in [V.I. Talyanskii, D.S. Novikov, B.D. Simons, L.S. Levitov, Phys. Rev. Lett. **87**, 276802 (2001)]. Such a setup could realize the quantum–mechanical version of an Archimedean screw that pumps on average a fraction of electron charge per cycle, operating by virtue of electron–electron interactions.

PACS numbers: 71.10.Pm, 85.35.Kt, 64.70.Rh

I. INTRODUCTION

Since their discovery¹, carbon nanotubes (NTs) remain in focus of both basic and applied research.^{2,3} Besides their important technological potential,^{4–8} nanotubes are a testing ground for novel physical phenomena involving strong electron interactions. Theoretically, they are considered perfect systems to study Tomonaga–Luttinger liquid effects.^{9–14} Experimentally, effects of electron–electron interactions in nanotubes have been observed in the Coulomb blockade peaks in transport,^{15,16} in the power law temperature and bias dependence of the tunneling conductance,^{17–19} as well as in the power law dependence of the angle–integrated photoemission spectra.²⁰

Remarkable features of carbon nanotubes allow one to study the ultimate consequence of strong electron–electron interactions, *Wigner crystallization*. The latter phenomenon has been in focus of experimental and theoretical efforts especially in two dimensional electron systems. Recent interest in this topic in the one–dimensional context has been stimulated by the conductance measurements in quantum wires and by possible importance of this phenomenon in transport.²¹ Carbon nanotube setup is in many respects ideal to study this phenomenon. Indeed, one–dimensional nature of the system increases interaction effects; the Dirac nature² of the single particle spectrum allows for essentially *exact* bosonized treatment

of electron–electron interactions via the massive Thirring – quantum sine–Gordon duality,^{22,23} spin and graphite Brilloin zone degeneracy² result in the presence of the *four* types of Dirac fermions with approximate $SU(4)$ symmetry of the problem that allows one to realize spin chains of high symmetry;¹³ robust chemical and mechanical NT properties result in very low disorder; finally, diverse methods of nanotube synthesis, a variety of available nanotube chiralities and of the ways of coupling to the nanotube electron system allow one to explore a wide region of the phase diagram.

In the present work we show that coupling of an external periodic potential to the nanotube electronic system can be used as a probe of electron correlations and interactions. We focus on the electron properties of single–walled carbon nanotubes in a periodic potential whose period λ_{ext} is much greater than the NT radius a , $\lambda_{\text{ext}} \gg a$. Such a potential can be realized using optical methods, by gating, or by an acoustic field. In all of these cases, realistic period λ_{ext} is of the order $0.1\text{--}1\ \mu\text{m}$. As shown below, effects of the Tomonaga–Luttinger correlations, realization of the $SU(4)$ invariant spin excitations, as well as the Wigner crystallization effects can be demonstrated in such a setup depending on the applied potential and on the NT parameters. Our main finding is the devil’s staircase of *incompressible electron states* whose existence relies on electron–electron interactions.

Below we will identify incompressible electron states

that arise when the NT electron number density ρ (counted from half-filling) is *commensurate* with the potential period:

$$\rho = \frac{m_{\text{tot}}}{\lambda_{\text{ext}}} , \quad m_{\text{tot}} = 4m . \quad (1)$$

In Eq. (1) m is the number of fermions of each of the four types (called below “flavors”) per potential period λ_{ext} .

In the absence of interactions, the Bloch theory only allows for the incompressible states in which the density (1) corresponds to *integer* m . These states are the result of the Bragg diffraction of the non-interacting electrons on the periodic external potential. As a result of this diffraction, *minigaps* in the single electron spectrum open²⁴ when $m = 0, \pm 1, \pm 2, \dots$.

In the present work we will show that electron-electron interactions result in additional incompressible states that arise at any *rational* $m = p/q$. In such a state, the NT electron system is locked by the periodic potential into a $q\lambda_{\text{ext}}$ -periodic structure sketched in Fig. 1. Naturally, the states with the lower denominator q will be more pronounced. Realistically, due to the finite system size and finite temperature, only a few states with small enough q could be reliably detected. However, these fractional- m states are very important. Minigaps that correspond to them are interaction induced and vanish in the noninteracting limit. Therefore, if measured, such minigaps would provide a direct probe of the strength of interactions between the NT electrons.

Quantum mechanical character of the problem and importance of electron-electron interactions in one dimension can be adequately addressed using the bosonized description of the NT electrons.^{10,11} In this case an electron is represented by a soliton of the corresponding bose field.¹⁴ Due to the presence of four flavors of electrons in a nanotube near half-filling, one obtains four bosonic modes that interact with each other.^{10,11,13} In the present work we develop a formalism that takes into account interaction between solitons of different flavors with the external periodic potential non-perturbatively.

We find that coupling of the periodic potential to the NT electron system allows one to distinguish between the two regimes for the ground state of interacting NT electrons: the four-flavor Luttinger liquid and the Wigner crystal.

In the stand-alone tube, one distinguishes between the two limits depending on how strongly electron wave functions are localized compared to the mean interparticle separation ρ^{-1} . This depends on the *curvature* of the Dirac electronic dispersion that is controlled by the NT gap at half-filling. Qualitatively, when electronic dispersion is approximately linear, electronic wavefunctions heavily overlap and the system is in the Luttinger liquid regime with four bosonic modes corresponding to NT electron flavors. The opposite limit of the Wigner crystal is realized when the size of the quantum sine-Gordon soliton representing electron is smaller than average interparticle separation. These two regimes are separated

by a *crossover* due to absence of phase transitions in one dimension.

External periodic potential introduces additional length scale, its period λ_{ext} , that naturally distinguishes between the two limits.

When the potential period is smaller than the size of the sine-Gordon soliton, the system is adequately described by the four flavor Luttinger liquid with a small gap. Although electron-electron interactions can be strong, it is the kinetic energy that dominates the physics. In this limit the external periodic potential opens minigaps in the spectrum due to the Bragg diffraction. We refer to this situation as to the *weak coupling limit* of the NT electrons to the external potential.

The opposite limit of the *strong coupling* is realized when the external periodic potential locks the Wigner crystal of semi-classical electrons. This happens when the size of the electron wave function (soliton size) is smaller than the potential period λ_{ext} . In this case fermionic exchange becomes unimportant due to small overlap of electronic wavefunctions. We find that the system of four flavors effectively behaves as the one of a *single* flavor with the total density (1). This happens since electrons of the same and of the different flavors avoid each other in a similar fashion due to the Coulomb repulsion rather than due to the Pauli principle. (Physically similar situation emerged in the context of the Hubbard model of spin- $\frac{1}{2}$ fermions in the works of Ogata and Shiba²⁵ and Cheianov and Zvonarev²⁶.) Not surprisingly, in this case energy gaps of the corresponding commensurate states are determined by the *total* density m_{tot} (that can be either integer or a simple fraction). We find a devil’s staircase of incompressible states in this limit.

How can the incompressible states be detected? One answer to this question was suggested in the recent proposal²⁴ of the nanotube adiabatic charge pump. In this setup the acoustoelectric effect in a NT in the presence of a surface acoustic wave (SAW) was suggested as a vehicle to realize adiabatic charge transport. A SAW propagating in the piezoelectric substrate is accompanied by a wave of charge density that results in the electric coupling between the SAW and the NT electrons. With the chemical potential inside one of the integer- m minigaps open due to the Bragg diffraction, the slowly moving SAW is predicted to induce *quantized current* in the nanotube, thus realizing the well-known Thouless pump.²⁷ An important observation made in Ref. 24 is that electron-electron interactions facilitate adiabaticity of the Thouless pump by effectively *increasing* the minigaps.

To detect incompressible electron states, including the ones with fractional m that were left out in Ref. 24, one can utilize the proposed adiabatic pumping setup. The latter could either employ surface acoustic waves as proposed in Ref. 24, or *e.g.* sequentially modulated voltages on the one dimensional periodic array of gates underneath the tube. When the chemical potential is inside the fractional- m minigap, the adiabatic current will cor-

respond to pumping of the *fractional charge per cycle*. Thus the presence of electron interactions can allow one to realize adiabatic pumping of charge (“Archimedean screw”) with the frequency that is a fraction of the frequency of the potential modulation.

This paper is organized as follows.

In the next Section we discuss the nature of incompressible states qualitatively and outline our main results.

In Section III we introduce the model Hamiltonian. In Section IV as a warm-up we consider the noninteracting problem. In Section V we bosonize the many-body Hamiltonian introduced in Section III.

Section VI is central. There, we introduce the phase soliton approach for the nanotube electrons in the periodic potential utilizing the bosonized description. We show how the weak or the strong coupling regime is selected depending on the saddle point of the total action for the four bosonic modes. We also discuss the role of quantum fluctuations.

Weak and strong coupling regimes are considered correspondingly in Sections VII and VIII. In Section IX we outline and discuss the phase diagram in the semiclassical (strong coupling) limit.

In Section X we discuss the adiabatic current setup as a means to observe incompressible states, and in Section XI we summarize our results.

II. QUALITATIVE CONSIDERATIONS AND OVERVIEW OF THE RESULTS

Below we will discuss the physics behind the incompressible states qualitatively, as well as briefly outline the approach adopted in the present work and our main results.

A. Incompressible states induced by electron interactions

Since interaction-induced incompressible electron states are the most important finding of the present paper, let us first give simple physical reasons for their existence.

First, consider a *classical* problem of the interacting 1D electrons of density (1) in a periodic potential. This is a typical example of the well studied problem of classical commensurate–incommensurate transitions (see e.g. the review²⁸). In this system incompressible charge states appear when the periodic electron configuration is locked by the periodic potential. This happens when the electron density (1) is commensurate with the potential period, i.e. $m_{\text{tot}} = 1/2$ is either integer or a simple fraction. An example of such a state with $m_{\text{tot}} = 1/2$ is shown schematically in Fig. 1(a).

The Dirac nature of carbon nanotubes brings about a set of incompressible states in which the Dirac “vacuum” is broken by a large potential amplitude. In this case the same total density $m_{\text{tot}} = n_e - n_h$ can be characterized by specifying the pair of numbers (n_e, n_h) of

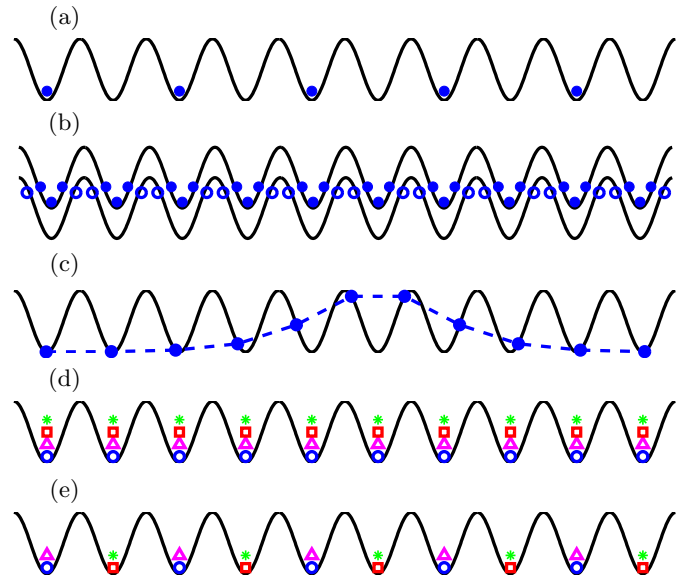


FIG. 1: Incompressible electron states (schematic). (a) The $(1/2, 0)$ state with $m_{\text{tot}} = 1/2$. (b) The $(3, 2)$ state with $m_{\text{tot}} = 1$. Large potential amplitude breaks the Dirac “vacuum” placing holes (open circles) into the potential maxima. (c) An example of the *phase soliton excitation* over the $(1, 0)$ state. Excitation gap is given by the phase soliton energy. (d) The $m = 1$ incompressible state that is allowed by the Bloch theory of non-interacting nanotube electrons. Four kinds of labels mark centers of the solitons of the bose fields that correspond to the NT fermions of the four flavors. (e) The simplest interaction-induced $m = 1/2$ state. In the weak coupling limit fermionic exchange is important. It is manifest by the solitons of the same flavor avoiding each other in every potential minimum due to the Pauli principle.

electrons and holes in the potential minima and maxima correspondingly. An example of the $(3, 2)$ state with $m_{\text{tot}} = 1$ is schematically shown in Fig. 1(b). In the ideal system, each commensurate state [with rational (n_e, n_h)] is *incompressible* (i.e. characterized by a finite excitation gap) since it costs a finite energy to add one more particle to the system. This energy can be estimated as that of a *phase soliton* that describes the distortion of the regular periodic charge configuration, as illustrated for the $(1, 0)$ state in Fig. 1(c).

Representing an excitation in a commensurate phase by a phase soliton was utilized in the past in various contexts. The model of locking a system into a commensurate state was first suggested in the work of Frenkel and Kontorova.²⁹ Later, it was re-discovered and solved by Frank and van der Merwe³⁰ in the context of atoms ordering on crystal surfaces, and by Dzyaloshinskii³¹ describing a transition to the state with a helical magnetic structure. The general theory of commensurate–incommensurate phase transitions has been finalized by Pokrovsky and Talapov.³²

A novel important feature of the problem with the nanotube electrons in the periodic potential is the presence of the *four* types (“flavors”) of the Dirac fermions.

It arises due to the spin and the Carbon Brilloin zone valley degeneracy of the effective NT Hamiltonian near half-filling². The problem possesses an approximate SU(4) symmetry in the space of the fermion flavors.^{13,24} The latter becomes exact¹³ in the forward scattering approximation^{9–11} that discards the coupling between the Brilloin zone valleys.

In this paper we will treat electron–electron interactions in the Luttinger liquid framework. In the bosonized picture¹⁴, an incompressible state corresponds to the lattice of the quantum sine–Gordon solitons of the bose–fields, that is commensurate with the external potential. Such a state is characterized by an average number m of solitons of each flavor per potential period λ_{ext} , in accord with Eq. (1). In Fig. 1(d,e) centers of solitons that represent electrons of different flavors are marked by different symbols. We estimate excitation gaps using the phase soliton approach that describes a distortion of such a soliton lattice over a length scale greater than its period [as shown schematically in Fig. 1(c)].

The SU(4) symmetry brings about an important simplification. In the bosonized language it results in only *two* different kinds of modes^{13,24}: the charge mode θ^0 and the three neutral flavor modes θ^a , $a = 1, 2, 3$. When the Coulomb repulsion is strong, the charge mode is stiff, whereas the flavor modes remain soft. As a consequence, *two* soliton length scales emerge, l_{ch} and l_{fl} , with l_{ch} corresponding to the stiff charge mode, and l_{fl} to the three neutral flavor modes whose quantum fluctuations renormalize effective couplings^{13,24}. When the electron interactions are strong, $l_{\text{ch}} \gg l_{\text{fl}}$.

In the absence of external potential, the ground state of the nanotube electron system was studied in the work of Levitov and Tsvelik.¹³ There, it was shown that the charged excitation of the minimal energy is a *composite soliton* in which the charge field θ^0 varies on the scale l_{ch} and the flavor fields θ^a vary on the scale l_{fl} . In this picture, the classical coordinate of an electron corresponds to the center of the composite soliton. Effects of exchange correspond to overlap of the flavor soliton cores of the composite solitons, whereas the Coulomb interaction is represented by the overlap of the charge solitons. At finite electron density the ground state is a compressible lattice of such composite objects.

When effects of exchange are small, the lattice of composite solitons of Levitov and Tsvelik describes the semi-classical one-dimensional Wigner crystal. This happens when the interparticle separation is greater than the flavor soliton size, $\rho^{-1} \gg l_{\text{fl}}$. Since there is no phase transition in one dimension, the crossover between the limits of the Luttinger liquid of delocalized electrons ($\rho^{-1} \ll l_{\text{fl}}$) and of the semi-classical Wigner crystal ($\rho^{-1} \gg l_{\text{fl}}$) happens smoothly, although physically these limits are very different. One or the other limit is selected by the *saddle point* of the bosonized action for the four modes. Levitov and Tsvelik considered this saddle point in the limit $\rho^{-1} \gg l_{\text{fl}}$ and determined the system’s compressibility. We underline that the Wigner crystallization as described

here occurs essentially due to having a finite *curvature* of the Dirac dispersion for the NT electrons. This curvature is controlled by the NT gap at half-filling. In the absence of this gap (e.g. in the case of the “armchair” tube) the system remains in the delocalized state described by the scale-invariant Luttinger liquid theory *regardless* of the strength of Coulomb repulsion between electrons.

Adding the periodic external potential does two things. First, it modifies the Dirac backscattering (within each Brilloin zone valley) thus changing soliton sizes l_{fl} and l_{ch} . Second, it *locks* the system into an incompressible state when the electron density (1) is commensurate with the potential period. In accord with the above, this locking is only possible when the curvature of the Dirac electron dispersion (NT gap at half-filling) is nonzero. This curvature gives rise to the finite soliton scales l_{ch} and l_{fl} . For the case of strictly linear dispersion (as in the armchair nanotube) both of these soliton sizes are formally infinite. In this limit minigaps due to the external periodic potential do *not* open. Technically, zero Dirac gap allows one to gauge the external potential away.

Depending on whether the NT electron wavefunctions (represented by solitons) overlap or are localized in the presence of the external periodic potential, we distinguish between the weak and the strong coupling limits mentioned in Introduction. These limits can be roughly defined by comparing the mean same-flavor fermion separation $4\rho^{-1} = \lambda_{\text{ext}}/m$ [cf. Eq. (1)] to the flavor soliton size l_{fl} determined self-consistently (more precise definitions will be deferred to Section VI). We thus consider the *weak coupling limit*, when

$$\lambda_{\text{ext}}/m \ll l_{\text{fl}}, \quad (2)$$

and the *strong coupling limit*, when

$$l_{\text{fl}} \ll \lambda_{\text{ext}}/m. \quad (3)$$

Below we briefly outline the results for each of these limits, postponing calculations to the remainder of the paper.

B. Weak coupling limit

In the regime (2) electron wavefunctions are sufficiently delocalized. Effects of fermionic exchange are important; in the bosonized language they correspond to the strong overlap of the *flavor* soliton cores. The system’s properties are dominated by the kinetic energy, with incompressible states appearing due to the Bragg diffraction of the delocalized wave packets on the external periodic potential. The fermion backscattering in this limit is small, and the minigaps that correspond to the commensurate states occupy a small part of the spectrum.

The presence of the flavor sector leads to the two energy scales Δ_{ch} and Δ_{fl} corresponding to the energies of the charged and of the neutral (flavor) excitations. When the Coulomb interaction is strong, $\Delta_{\text{ch}} \gg \Delta_{\text{fl}}$, and the excitation gap is dominated by Δ_{ch} .

In Section VI below we develop the general procedure of how to estimate the excitation gap for the $m = p/q$ commensurate state. For that we generalize the phase soliton approach³² to the quantum mechanical case of the four modes.

Let us briefly outline the main steps of this procedure. Starting from the fully bosonized Lagrangian $\mathcal{L}[\theta^0, \theta^a]$ for the four bosonic modes derived in Section V, one develops the perturbation theory in the small backscattering g_0 that is proportional to the bare NT gap Δ_0 , $g_0 \propto \Delta_0$ [Eq. (45)], to derive the effective Lagrangian $\mathcal{L}_m[\bar{\theta}^0, \theta^a]$ for the “slow” *phase modes*. The latter are constant in the commensurate state characterized by the density (1). The excitation gap in this language is dominated by the energy of the charge soliton governed by the effective phase mode Hamiltonian

$$\mathcal{H}_m[\bar{\theta}^0] = \text{const.} \int dx \left\{ \frac{K}{2} (\partial_x \bar{\theta}^0)^2 + g_m^* \cos(\beta \bar{\theta}^0) \right\} \quad (4)$$

for the charged phase mode $\bar{\theta}^0$. Here the coefficient β and the constant in front depend on the normalization of the charge mode, $K \geq 1$ is the charge stiffness ($K = 1$ in the noninteracting limit), and g_m^* is the backscattering renormalized by quantum fluctuations of the flavor sector. Its bare value $g_m \propto g_0^q$ depends on the bare Dirac gap, on the electron density $m = p/q$ according to Eq. (1), as well as on the form of the external periodic potential.

In the present work we will realize the outlined program in Section VII. There, in Sec. VII A we consider in detail the integer- m case of Ref. 24, where the phase soliton analysis is trivial, $g_m \propto g_0$. We note that the integer- m case in the weak coupling limit is adiabatically connected to the single particle Bragg diffraction of non-interacting electrons of four flavors on the periodic potential, in which case minigaps *do open* [Section IV]. We will also show that the corresponding minigaps are strongly enhanced by the repulsive electron interactions²⁴.

Later, in Sec. VII B we will derive the Lagrangian $\mathcal{L}_{1/2}[\bar{\theta}^0, \bar{\theta}^a]$ [Eqs. (112) and (113)] and the effective Hamiltonian of the form (4) [Eq. (122)] for the simplest *fractional- m* case of $m = 1/2$. In particular, we will obtain the coupling $g_{1/2}^* \propto (K-1)^2/K^2$ [Eq. (121)]. In the limit of strong electron repulsion $K \gg 1$ the charge excitation gap [Eq. (123)] is large scaling as $\Delta_{1/2} \propto \sqrt{K}$, whereas in the nointeracting limit $K = 1$ this gap vanishes as expected according to the Bloch theory.

Finally, both for the integer- m case and for $m = 1/2$ we will show that the excitations of the *flavor* sector are governed by the effective O(6) Gross–Neveu model on the energy scale $\Delta_{\text{fl}} \sim K^{-1/2} \Delta_{\text{ch}}$.

C. Strong coupling limit

In the regime (3) the system’s properties are dominated by the potential energy, whereas the effects of the exchange become unimportant. Technically, this limit corresponds to the flavor solitons being sharp kinks on the

scale l_{ch} and λ_{ext} , with exponentially small overlap (exchange). In this regime, the Dirac gap Δ is large which results in the gaps occupying a substantial part of the spectrum.

In contrast to the perturbative limit (2), in the regime (3) we find that the original NT electrons of four flavors effectively behave as a system of fermions of a *single flavor* with the total density (1). This can be understood with the help of the following simple observation: In the case of large Coulomb repulsion, fermions of different flavors avoid each other as strongly due to interactions as they avoid those of the same flavor due to the Pauli principle.

Although in the limit (3) exchange effects are small, the role of the flavor sector is significant. First, the soft flavor degrees of freedom adjust themselves to provide an effective potential for the stiff charge mode θ^0 in a way similar to that described in Ref. 13. Such an adjustment occurs in every minimum of the external potential and is an effect non-perturbative in backscattering g_0 . Second, quantum fluctuations of the flavor sector renormalize the effective parameters and result in the universal scaling exponent 4/5 for the renormalized backscattering (Dirac gap) in the limit of infinitely strong electron repulsion.^{13,24}

We consider the strong coupling limit in detail in Section VIII. Focussing on the system’s properties on the energy scale of the charge sector $\Delta_{\text{ch}} \gg \Delta_{\text{fl}}$ we keep only the charged mode in the effective Lagrangian [Eq. (125)], in which the neutral modes have resulted in the effective potential for the charged sector and in the renormalized couplings. Re-fermionizing this Lagrangian we obtain the effective Hamiltonian for the *spinless* Dirac fermions [Eq. (132)] with renormalized parameters, in the presence of the external periodic potential. This Hamiltonian allows one to apply the phase soliton approach for the *single mode* in order to find the excitation gaps [Eq. (140)] that in this limit depend on the *total density* $m_{\text{tot}} = 4m$ defined according to Eq. (1).

Finally, in the Section IX we consider the semi-classical limit of the problem to draw the phase diagram. In this limit the Wigner crystal of the NT electrons is locked by the external periodic potential. We outline the phase diagram using the classical limit of the effective single-mode Hamiltonian (132). This diagram (Fig. 7) has a structure of the devil’s staircase.

III. THE MODEL

In the present Section we outline the model of interacting nanotube electrons coupled to the external periodic potential. We first briefly introduce the Dirac nanotube Hamiltonian near half-filling in the effective mass approximation, then describe coupling of the NT electrons to the external potential, and finally introduce the model that takes into account the Coulomb repulsion between electrons. This model will have an approximate SU(4)

symmetry in the space of the fermion “flavors” that we will use in the remainder of this work.

A. Nanotube phenomenology

A remarkable feature of Carbon nanotubes is the Dirac symmetry of their electronic spectrum near half-filling². It stems from the semimetallic character of the two-dimensional Carbon monolayer (so-called graphene sheet), whose valence and conduction bands touch each other at the two inequivalent (K and K') points of the Brilloin zone. These points are separated by a large wave vector $K_{BZ} \sim 1/a_{cc}$, where $a_{cc} = 0.143$ nm is the length of the Carbon bond. DiVincenzo and Mele³³ made an important observation that the electron spectrum of a graphene sheet near both K and K' points in the tight-binding approximation is described in terms of the 2D massless Dirac fermions. A nanotube can be viewed as a wrapped Carbon monolayer. Depending on the NT type, such a wrapping imposes a (quasi)periodic boundary condition on the graphene electrons that may or may not produce an effective mass for the resulting 1D NT fermions. In general, the NT low energy spectrum is controlled by the 1D *massive* Dirac fermions near each of the two Dirac points.² In this work we choose the basis (with x along the tube) in which the Dirac Hamiltonian near the K or K' point has the following form:

$$\mathcal{H}_D = -i\hbar v \sigma_3 \partial_x + \Delta_0 \sigma_1. \quad (5)$$

The Hamiltonian (5) is written in the Weyl basis where the components of the wave function $\psi = (\psi_R \ \psi_L)^T$ represent the right and left moving particles. Here $\sigma_{1,3}$ are the Pauli matrices and $v \approx 8 \cdot 10^7$ cm/s is the NT Fermi velocity. The Hamiltonian (5) yields the Dirac dispersion

$$\epsilon^2(p) = p^2 v^2 + \Delta_0^2 \quad (6)$$

where the momentum $p \ll \hbar/a_{cc}$ is measured with respect to the NT Dirac points.

Depending on the NT type, a wide range of values for the Dirac gap Δ_0 is available².

Semiconducting nanotubes have a large gap

$$\Delta_0^{(\text{semicond.})} = \frac{\hbar v}{3a} \simeq 0.18 \text{ eV}/a_{[\text{nm}]} \quad (7)$$

that is inversely proportional to the NT radius a .

Metallic NTs can be of the two kinds. There are truly metallic, or the so-called “armchair” NTs which have a zero gap at half-filling, $\Delta_0 = 0$. However, a gap

$$\Delta_0 \ll D \quad (8)$$

that is small compared to the 1D bandwidth

$$D = \frac{\hbar v}{a} = 0.53 \text{ eV}/a_{[\text{nm}]} \quad (9)$$

can appear due to the curvature of the 2D graphene sheet in the nominally metallic tube. This gap is inversely proportional to the square of the NT radius, and is numerically given by

$$\Delta_0^{(\text{semimet.})} \approx 10 \text{ meV} \cdot |\cos 3\Theta_{\text{ch}}|/a_{[\text{nm}]}^2 \quad (10)$$

as a function of the NT *chiral angle* Θ_{ch} .^{34,35} Even smaller Δ_0 can be induced in a strictly metallic “armchair” ($\Theta_{\text{ch}} = \pi/6$) tube by applying magnetic field parallel to the NT axis.^{36,37}

B. Coupling to external potential

In the present work we consider the nanotube subject to the external periodic potential which for the purpose of simpler algebra we take to be a harmonic function,

$$U(x) = A \cos k_{\text{ext}} x, \quad k_{\text{ext}} = 2\pi/\lambda_{\text{ext}}. \quad (11)$$

Qualitatively, the results of this work will be valid for any periodic potential realized by the means described in the Introduction.

As mentioned in Secion I, realistic values of the period λ_{ext} are in the $0.1 - 1 \mu\text{m}$ range. The separation of scales $k_{\text{ext}} \ll 1/a \ll 1/a_{cc}$ results in the following important simplification. Focussing on the lowest Dirac subband (near half-filling), we discard the coupling between the K and K' points in the Brilloin zone since these processes involve momentum transfer $\sim 1/a_{cc} \gg k_{\text{ext}}$. Also, in this work we do not consider effects of external magnetic fields. The electrostatic potential (11) couples to the total charge density and therefore does not distinguish between spin polarizations.

As a result, in the absense of electron-electron interactions, we effectively have four ($2_{\text{spin}} \times 2_{\text{valley}}$) decoupled fermion types, which we call “flavors”, each described by the same Dirac equation

$$\{\mathcal{H}_D + U(x)\} \psi = \epsilon \psi, \quad (12)$$

where \mathcal{H}_D is given by Eq. (5).

Coulomb interaction couples the four electron flavors as described below.

C. Interacting NT electrons in the forward scattering approximation

In what follows we will work in the *forward scattering approximation* established for the nanotubes in Refs. 10 and 11. According to the latter, even in the presence of electron interactions, the two inequivalent Dirac points in the Carbon Brilloin zone (mentioned above in Sec. III A) remain approximately decoupled. As a result, near half filling, nanotubes can be approximately described by the following second-quantized Hamiltonian,

$$\mathcal{H} = \mathcal{H}_0 + \mathcal{H}_{\text{bs}} + \mathcal{H}_{\text{ext}}. \quad (13)$$

The first term \mathcal{H}_0 is the massless Dirac Hamiltonian with the Coulomb interaction between the four fermion flavors:

$$\mathcal{H}_0 = -i\hbar v \int \sum_{\alpha=1}^4 \psi_{\alpha}^+ \sigma_3 \partial_x \psi_{\alpha} dx + \frac{1}{2} \sum_k \rho_k V(k) \rho_{-k} . \quad (14)$$

Here

$$\psi_{\alpha} = \begin{pmatrix} \psi_{\alpha}^R \\ \psi_{\alpha}^L \end{pmatrix} , \quad 1 \leq \alpha \leq 4 \quad (15)$$

is a two component Weyl spinor of the flavor α , and

$$\rho(x) = \sum_{\alpha=1}^4 \psi_{\alpha}^+ (x) \psi_{\alpha}(x) \quad (16)$$

is the total charge density in which we neglected the strongly oscillating components $\sim e^{\pm 2iK_{\text{BZ}}x}$, with $K_{\text{BZ}} \sim 1/a_{\text{cc}}$ defining the position of the Dirac points in the Brilloin zone of graphene. For a nanotube of a radius a placed on a substrate with the dielectric constant ε , the 1D Coulomb interaction

$$V(k) = \frac{2}{\varepsilon+1} V_0(k) , \quad (17)$$

where

$$V_0(k) \simeq e^2 \ln [1 + (ka)^{-2}] . \quad (18)$$

In writing the Hamiltonian (14) we have discarded the backscattering and Umklapp processes between the *different* Dirac points of the graphene Brilloin zone. These processes are small in $a_{\text{cc}}/a \lesssim 0.1$, with $a_{\text{cc}} = 0.143$ nm being the length of the Carbon bond (Sec. IV). The Umklapp amplitude is also shown to be small numerically¹². Since the long range potential (17) does not discriminate between the Carbon sublattices, scattering amplitudes for the fermions of same and opposite chiralities at each Dirac point are equal^{10,11}. This naturally leads to the approximation in which electron interaction in Eq. (14) only involves the smooth part (16) of the total electron density.

The second term in the Hamiltonian (13) describes the backscattering between the left and right moving fermions *within* each Dirac point:

$$\mathcal{H}_{\text{bs}} = \Delta_0 \int \sum_{\alpha=1}^4 \psi_{\alpha}^+ \sigma_1 \psi_{\alpha} dx . \quad (19)$$

The bare gap Δ_0 can originate due to any of the reasons outlined in Section III A above.

Finally, interaction with the external periodic potential is represented by

$$\mathcal{H}_{\text{ext}} = \int dx \rho U(x) , \quad (20)$$

where we use the model potential U defined in Eq. (11).

The Hamiltonian (13) written in the forward scattering approximation is SU(4) invariant with respect to rotations in the space of the four fermion flavors ψ_{α} .

IV. NONINTERACTING ELECTRONS

In the present Section we consider single electron spectrum (12) of a Carbon nanotube in a periodic potential. This simple problem is instructive since it allows us to identify the two regimes of coupling of a NT electron to the external potential in the noninteracting case. They are the limit of nearly free electrons, and the tight-binding limit. To distinguish between them, we compare the size of the single electron wavefunction l_{wf} with the period of the potential λ_{ext} . These two regimes are to a great extent parallel to, correspondingly, the weak and the strong coupling limits of the fully interacting problem, where one draws the distinction by comparing the quantum sine-Gordon soliton size to λ_{ext} .

To analyze the energy spectrum of the single particle problem (12) quantitatively we will follow the approach taken in Ref. 24 and will reproduce some of its results which we will need below. It is convenient to perform a gauge transformation

$$\psi'(x) = e^{-i\bar{A}\sigma_3 \sin k_{\text{ext}} x} \psi(x) , \quad (21)$$

where we introduced the dimensionless potential amplitude

$$\bar{A} = \frac{A}{\epsilon_0} . \quad (22)$$

The energy scale

$$\epsilon_0 \equiv \hbar k_{\text{ext}} v = \hbar v / \lambda_{\text{ext}} = 3.3 \text{ meV} / \lambda_{\text{ext}} [\mu\text{m}] \quad (23)$$

is a natural measure of the relevant energies and it will be utilized throughout this work. The energy ϵ_0 has a meaning of the Dirac particle-in-the-box energy quantization in each potential minimum. It is a relative measure of the kinetic energy per potential period.

After the gauge transformation (21) the Hamiltonian $\mathcal{H}_D + U(x)$ becomes

$$\mathcal{H}' = -i\hbar v \partial_x \sigma_3 + \Delta_0 \sigma_1 e^{-2i\bar{A}\sigma_3 \sin k_{\text{ext}} x} . \quad (24)$$

Note that due to the Dirac character of the problem, in the Hamiltonian (24) the relative importance of the potential energy (the second term) is governed by the value of the Dirac gap Δ_0 (rather than the potential amplitude A), whereas the kinetic energy (the first term) is of the order ϵ_0 .

Due to a variety of the available Dirac gap values Δ_0 , the coupling of the NT electron to the external potential can be either weak or strong. Consider the eigenvalue problem

$$\mathcal{H}' \psi' = \epsilon \psi' \quad (25)$$

that is periodic in λ_{ext} . Its solutions are the spinor Bloch states $\psi_p(x) = u_p(x) e^{ipx}$ with a quasimomentum $\hbar p$ taking values in the effective Brillouin zone defined by the potential period, $-k_{\text{ext}}/2 < p < k_{\text{ext}}/2$. We distinguish

between the weak coupling limit (nearly free electrons) and the strong coupling (tight binding) limit by comparing the size l_{wf} of the single particle spinor wavefunction $u_p(x)$ with the period λ_{ext} of the potential. The length scale l_{wf} in general depends on the quasimomentum p , on the backscattering Δ_0 and on the profile and strength of the external potential.

In the limit of *nearly free electrons*

$$\lambda_{\text{ext}} \ll l_{\text{wf}}. \quad (26)$$

In this case the electron wave functions are close to plane waves. As shown in Ref. 24, diffraction on the periodic potential results in mixing between the left and right moving states of the Dirac spectrum at particular values of the electron quasimomentum, opening minigaps in the single particle spectrum.

An opposite regime is the *strong coupling*, or the *tight-binding limit*

$$l_{\text{wf}} \leq \lambda_{\text{ext}}, \quad (27)$$

in which case the external potential localizes the semi-classical Dirac electrons (holes) in its minima (maxima). In this case the corresponding minigaps become larger than subbands.

Below we consider the two limits separately.

A. Nearly free electrons, $\lambda_{\text{ext}} \ll l_{\text{wf}}$

Consider first the case $\Delta_0 = 0$, in which $u_p = \text{const}$ and, formally, $l_{\text{wf}} = \infty$. One can readily see from Eq. (24) that in the absence of electron backscattering the external potential is gauged away and does not affect the spectrum. This is a manifestation of the fact that the scalar external potential does not mix massless Dirac branches whose wave functions have a spinor structure. The other way of understanding it is that, in agreement with the discussion after Eq. (24), the potential energy has a relative scale determined by the backscattering Δ_0 , and vanishes when $\Delta_0 = 0$.

In the presence of small backscattering the problem was solved in Ref. 24 by treating the potential term in Eq. (24) as a perturbation. This perturbation mixes right and left moving spectral branches at the momenta values

$$p_m = \pm \frac{m}{2} k_{\text{ext}}, \quad m = \pm 1, \pm 2, \dots. \quad (28)$$

Using the Fourier decomposition

$$e^{-iz \sin k_{\text{ext}} x} = \sum_{m=-\infty}^{\infty} J_m(z) e^{-imk_{\text{ext}} x}, \quad (29)$$

where J_m are the Bessel functions and $z = 2\bar{A}$, minigaps of the size

$$\Delta_m^{(0)}(\bar{A}) = \Delta_0 |J_m(2\bar{A})| \quad (30)$$

open up at the energy values $\epsilon_m = m\epsilon_0/2$. The superscript (0) in Eq. (30) relates to the noninteracting case considered in the present Section. Minigaps (30) oscillate as a function of the potential amplitude A and vanish for particular values of A corresponding to zeroes of the Bessel functions.

B. Tight binding limit $l_{\text{wf}} \leq \lambda_{\text{ext}}$

Now let us consider the tight binding case (27) when the sub-bands become exponentially narrow.

In this regime the spectrum can be obtained by solving the problem (25) numerically via the transfer matrix approach outlined in Ref. 24. For an illustration, below we consider the borderline case $\Delta_0 = \epsilon_0$ in which the potential and kinetic energy in the Hamiltonian (24) are of the same order. The spectrum is shown in Fig. 2 as a function of the potential amplitude A . Energy gaps oscillate as a function of A and vanish at particular amplitude values. The spectrum also has a characteristic Dirac $\epsilon \rightarrow -\epsilon$ symmetry.

Fig. 2 suggests that even for the case $\Delta_0 = \epsilon_0$ minigaps occupy most of the spectrum when $A \sim \epsilon_0$. In this case the electron dispersion in each miniband is almost flat. This corresponds to electrons and holes being localized in the minima and maxima of the external potential correspondingly, with an exponentially suppressed tunneling between the adjacent potential wells. Such a tight-binding regime is opposite to the case of nearly free electrons (26) with the minigaps (30).

Below we identify conditions for the tight binding limit (27). For that one needs to consider the two cases depending on the relation between the potential amplitude A and the mass term Δ_0 .

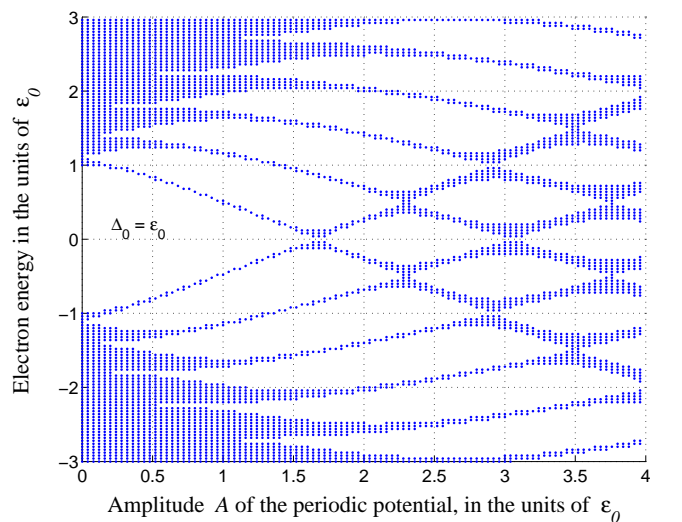


FIG. 2: Single electron spectrum for the nanotube in the presence of the external potential (11) for the case $\Delta_0 = \epsilon_0$, where ϵ_0 is defined in Eq. (23)

The case $A \ll \Delta_0$ corresponds to the “nonrelativistic limit” of the Dirac equation, where all the relevant energies are much smaller than the gap Δ_0 . We define the “Dirac” electron mass M as

$$\Delta_0 = Mv^2. \quad (31)$$

This allows for the Schrödinger description, in full analogy with the non-relativistic limit of the Dirac equation in quantum electrodynamics. The corresponding Hamiltonian

$$\mathcal{H}_{\text{Sch}} = -\frac{\hbar^2}{2M} \partial_x^2 + U(x). \quad (32)$$

Tunneling amplitude between the adjacent minima of $U(x)$ is proportional to $e^{-S|_{A < \Delta_0}/\hbar}$, where the classical action under the barrier

$$S|_{A < \Delta_0} = \frac{4\hbar\sqrt{A\Delta_0}}{\epsilon_0}. \quad (33)$$

Therefore both the minibands and tunneling are suppressed in the limit $A \ll \Delta_0$ if

$$\left(\frac{\Delta_0}{\epsilon_0}\right)^{-1} < \frac{A}{\epsilon_0} \ll \frac{\Delta_0}{\epsilon_0}. \quad (34)$$

The inherently Dirac regime occurs when $A > \Delta_0$. In this case electron can tunnel between the minima of the potential (11) sequentially through the hole part of the spectrum. The corresponding tunneling amplitude $\sim e^{-2S|_{A > \Delta_0}/\hbar}$, where the classical action under barrier between the electron and hole parts is

$$S|_{A > \Delta_0} = \frac{1}{v} \int dx \sqrt{|(E - U(x))^2 - \Delta_0^2|}. \quad (35)$$

Tunneling from the minimum of $U(x)$ at $E = \Delta_0 - A$ to the hole part of the spectrum yields ($\zeta \equiv \Delta_0/A$)

$$\begin{aligned} S|_{A > \Delta_0} &= \frac{2\hbar A}{\epsilon_0} \left\{ \sqrt{\zeta} - (1 - \zeta) \ln \frac{1 + \sqrt{\zeta}}{\sqrt{1 - \zeta}} \right\} \\ &= \frac{4\hbar\Delta_0^{3/2}}{\epsilon_0 A^{1/2}} \left(\frac{1}{1 \cdot 3} + \frac{\zeta}{3 \cdot 5} + \frac{\zeta^2}{5 \cdot 7} + \dots \right). \end{aligned} \quad (36)$$

Tunneling from the energy level $|E| \ll 2A$ far from the potential bottom yields the action $S \simeq \pi\Delta_0^2/\hbar v \mathcal{E}$, where $\mathcal{E} = |\partial_x U(x)|$. As a result we obtain that the single particle bandwidth in the Dirac regime is exponentially suppressed if

$$\frac{\Delta_0}{\epsilon_0} < \frac{A}{\epsilon_0} < \left(\frac{\Delta_0}{\epsilon_0}\right)^c, \quad (37)$$

where the exponent $c = 3$ for tunneling from the potential minimum and $c = 2$ for tunneling from energy level far from the potential bottom.

Summarizing, Eqs. (34) and (37) yield the following criterion for the tight-binding limit (27) in terms of the potential amplitude A :

$$\left(\frac{\Delta_0}{\epsilon_0}\right)^{-1} < \frac{A}{\epsilon_0} < \left(\frac{\Delta_0}{\epsilon_0}\right)^c, \quad \Delta_0 > \epsilon_0. \quad (38)$$

Increasing the potential amplitude A beyond $\Delta_0^c/\epsilon_0^{c-1}$ actually *enhances* the tunneling amplitude between the particle and hole continua. This is reflected in Fig. 2 by wider minibands for $A > \epsilon_0$. Indeed, an increase in A makes the tunneling barrier through the Dirac gap $2\Delta_0$ shorter, and reduces the action under the barrier. The other way of understanding the apparent delocalization of the wave functions for large A is to notice that large potential amplitude results in strong oscillations of the potential term in Eq. (24). These oscillations effectively average this term to zero in the limit $A \rightarrow \infty$, in which case the minigaps become small as $A^{-1/2}$. The latter follows from the large- A asymptotic behavior of the Bessel functions for the weak coupling minigaps (30) that become valid in this limit.

The picture described in the present Section does not take into account electron interactions that are crucial in one dimension. In the following Section we will introduce a bosonized description of interacting electrons in a nanotube. This framework will allow us to define the weak and the strong coupling limits for the *interacting* system in Section VI. There, the soliton size will play the role of l_{wf} .

V. BOSONIZATION

Below we will outline the bosonized description for the interacting NT electrons in the external field. Our treatment will be similar to that introduced in Refs. 24 and 13. For the sake of completeness we shall present it in detail. The formalism of the present Section will be used below in Sections VI, VII and VIII to study the effect of interactions on the energy spectrum.

We bosonize^{10,11,13,14} the Hamiltonian (13) by virtue of the massive Thirring – quantum sine-Gordon duality,^{22,23} by representing the fermionic operators (15) as nonlocal combinations of bose fields

$$\psi_\alpha = \frac{1}{\sqrt{2\pi a}} e^{i\Theta_\alpha}. \quad (39)$$

The conjugate momenta

$$\Pi_\alpha = \frac{1}{\pi v} \partial_t \Theta_\alpha \quad (40)$$

obey the usual canonical relations

$$[\Pi_\alpha(x), \Theta_\beta(y)]_- = -i\delta_{\alpha\beta} \delta(x - y). \quad (41)$$

As a result we obtain the Lagrangian

$$\mathcal{L} = \frac{\hbar v}{2\pi} \int dx \sum_{\alpha=1}^4 \left(\frac{1}{v^2} (\partial_t \Theta_\alpha)^2 - (\partial_x \Theta_\alpha)^2 \right) - \frac{1}{2} \sum_q \rho_{-q} V(q) \rho_q - \int dx \left(\frac{\Delta_0}{\pi a} \sum_{\alpha=1}^4 \cos 2\Theta_\alpha + \rho(x) U(x) \right) , \quad (42)$$

where the total charge density (1) in terms of the bosonic variables is given by

$$\rho(x) = \sum_{\alpha=1}^4 \rho_\alpha = \sum_{\alpha=1}^4 \frac{1}{\pi} \partial_x \Theta_\alpha . \quad (43)$$

The Lagrangian (42) corresponds to the sine-Gordon Hamiltonian for the four interacting bosonic fields Θ_α ,

$$\mathcal{H}_{\text{sG}}[\Theta_\alpha] = \frac{\hbar v}{\pi} \int dx \left\{ \frac{1}{2} \sum (\partial_x \Theta_\alpha)^2 + \frac{K-1}{8} \left(\sum \partial_x \Theta_\alpha \right)^2 + \frac{1}{4} g_0 \sum \cos 2\Theta_\alpha + \frac{1}{\hbar v} \sum \partial_x \Theta_\alpha \cdot (U(x) - \mu) \right\} . \quad (44)$$

Here the coupling (bare backscattering)

$$g_0 = \frac{4\Delta_0}{\hbar v a} = \frac{4}{a^2} \frac{\Delta_0}{D} , \quad (45)$$

where D is the bandwidth (9), μ is the chemical potential calculated from the half filling, and the charge stiffness

$$K_q = 1 + 4\nu V(q) , \quad \nu = \frac{1}{\pi \hbar v} . \quad (46)$$

Below we drop the (irrelevant) logarithmic dependence of the stiffness K_q on the momentum, assuming a constant value $K \equiv K_{q \sim 1/l_{\text{ch}}}$, where l_{ch} is the charge soliton length that is found in each specific case self-consistently. The meaning of l_{ch} is the length scale beyond which the

Coulomb interaction is screened; it depends on the distance to the metallic gate and at least cannot exceed the tube length L . Since the dependence of the stiffness K on l_{ch} is only logarithmic, using $e^2/\hbar v \simeq 2.7$ one can estimate $K \simeq 40$ for $l_{\text{ch}} \sim 1 \mu\text{m}$ for the stand-alone tube; if the tube is placed on the dielectric substrate with realistic dielectric constant $\varepsilon \simeq 10$, then $K \simeq 10$.

For the further analysis it is convenient to shift the displacement fields

$$\Theta_\alpha(x) \rightarrow \Theta_\alpha(x) - \frac{1}{\hbar v} \int^x K^{-1} (U - \mu) dx' . \quad (47)$$

This procedure is analogous to gauge transforming the fermion operators (21). The transformed Hamiltonian (44) is

$$\mathcal{H}'_{\text{sG}}[\Theta_\alpha] = \frac{\hbar v}{\pi} \int dx \left\{ \frac{1}{2} \sum (\partial_x \Theta_\alpha)^2 + \frac{K-1}{8} \left(\sum \partial_x \Theta_\alpha \right)^2 + \frac{1}{4} g_0 \sum_{\alpha=1}^4 \cos \left(2\Theta_\alpha + 2\tilde{\mu} k_{\text{ext}} x - 2\tilde{A} \sin k_{\text{ext}} x \right) \right\} , \quad (48)$$

where the dimensionless quantities

$$\tilde{A} = \frac{A}{K\epsilon_0} , \quad \tilde{\mu} = \frac{\mu}{K\epsilon_0} \quad (49)$$

are introduced in a way similar to that of Eq. (22), with the energy scale ϵ_0 defined in Eq. (23). The difference between Eqs. (49) and (22) is in additional *screening* (by a factor of $1/K$) of external fields $U(x)$ and μ by the interacting NT system.

There is an important relationship between the total density (1) or (43) and the chemical potential μ . It is convenient to express it in terms of the the number m of fermions of each flavor per potential period. In the absense of backscattering the connection between m and the screened dimensionless chemical potential $\tilde{\mu}$ is simple:

$$m = 2\tilde{\mu} . \quad (50)$$

When $g_0 = 0$, the fermion density m varies continuously with $\tilde{\mu}$. In this case, as we pointed out earlier in Section II, gaps do not open, and the system is a scale invariant Tomonaga–Luttinger liquid of four flavors regardless of how strong electron–electron repulsion is.³⁸

The latter statement becomes obvious after diagonalizing the Gaussian parts of the Lagrangian (42) and the Hamiltonians (44) and (48) by the unitary transformation^{13,24}

$$\begin{pmatrix} \Theta_1 \\ \Theta_2 \\ \Theta_3 \\ \Theta_4 \end{pmatrix} = \frac{1}{2} \begin{pmatrix} 1 & 1 & 1 & 1 \\ 1 & -1 & 1 & -1 \\ 1 & -1 & -1 & 1 \\ 1 & 1 & -1 & -1 \end{pmatrix} \begin{pmatrix} \theta^0 \\ \theta^1 \\ \theta^2 \\ \theta^3 \end{pmatrix} . \quad (51)$$

In the new variables the total charge density (43) reads

$$\rho(x) = \frac{2}{\pi} \partial_x \theta^0 . \quad (52)$$

Transformation (47) leaves θ^a intact, and shifts

$$\theta^0 \rightarrow \theta^0 - \frac{2}{\hbar v} \int^x K^{-1}(U - \mu) dx' . \quad (53)$$

Using the identity

$$\sum_{\alpha=1}^4 \cos 2\Theta_\alpha = 4\mathcal{F}(\theta^0, \theta^a) , \quad (54)$$

where

$$\mathcal{F}(\theta^0, \theta^a) = \cos \theta^0 \cdot \prod_{a=1}^3 \cos \theta^a + \sin \theta^0 \cdot \prod_{a=1}^3 \sin \theta^a , \quad (55)$$

as a result we obtain the Lagrangian^{13,24}

$$\mathcal{L}' = \mathcal{L}_0 + \mathcal{L}_{\text{bs}} \quad (56)$$

describing one stiff charge mode and three soft flavor modes, where

$$\begin{aligned} \mathcal{L}_0 &= \frac{\hbar v}{2\pi} \int dx \left(\frac{1}{v^2} (\partial_t \theta^0)^2 - K (\partial_x \theta^0)^2 \right) \\ &+ \frac{\hbar v}{2\pi} \int dx \sum_{a=1}^3 \left(\frac{1}{v^2} (\partial_t \theta^a)^2 - (\partial_x \theta^a)^2 \right) \end{aligned} \quad (57)$$

$$\mathcal{L}_{\text{bs}} = -\frac{\hbar v g_0}{\pi} \int dx \mathcal{F}(\theta^0 + 2\tilde{\mu}k_{\text{ext}}x - 2\tilde{A} \sin k_{\text{ext}}x, \theta^a) \quad (58)$$

The Gaussian Lagrangian \mathcal{L}_0 describes three flavor modes that move with velocity v , and one charge mode that has a strongly enhanced velocity

$$\bar{v} = K^{1/2}v . \quad (59)$$

This is a manifestation of the separation between charge and flavor in a strongly interacting system described by the Hamiltonian \mathcal{H}_0 . The interaction term (58) becomes relevant at certain electron densities and is responsible for incompressible states.

Note that the Lagrangians (42) and (56) are SU(4) invariant, as is the original Hamiltonian \mathcal{H} . This invariance is not explicit in the adapted notation. It will manifest itself below at the level of renormalization.

VI. PHASE SOLITON APPROACH FOR NANOTUBE ELECTRONS

The purpose of the present Section is to lay out the formalism that allows one to calculate excitation gaps for incompressible electron states. We will combine the bosonized description developed in the previous Section with the phase soliton approach.³² Our goals below will be to distinguish between the weak and strong coupling regimes and to generalize the phase soliton approach to the case of four modes.

In what follows, our analysis of the quantum problem will be based on finding the saddle point of the total

bosonized action $\mathcal{L}_m[\bar{\theta}^0, \bar{\theta}^a]$. It will be instructive to first consider the simpler saddle point found by Levitov and Tsvelik¹³ for the problem (56) in the absence of the external potential. Here we will focus on the “switching” of the soft flavor modes θ^a on the length scale l_{fl} . Such a switching optimizes effective potential for the stiff charge mode in the limit of strong electron repulsion $K \gg 1$.

Next we will consider the full problem (56). We will first demonstrate how incompressible states arise in the *classical* system by numerically minimizing the sine-Gordon Hamiltonian (44) for the density $m = 1/2$. Then, to study incompressible states analytically, we will introduce the phase soliton approach that allows one to obtain the effective Lagrangian $\mathcal{L}_m[\bar{\theta}^0, \bar{\theta}^a]$ for the slow phase modes. The charge phase mode Hamiltonian (4) will follow from the Lagrangian $\mathcal{L}_m[\bar{\theta}^0, \bar{\theta}^a]$ via the saddle-point optimization performed by the soft neutral sector. We will show that, in the presence of external periodic potential, such a saddle point depends on how sharply the flavor modes $\bar{\theta}^a$ “switch” on the scale on which the phase of the potential energy $\sim \cos \theta^0$ for the charged phase mode changes by 2π . Slow and fast switching are referred to as the weak and the strong coupling limits correspondingly. The final step in deriving the effective Hamiltonian (4) will be to take into account effects of quantum fluctuations of the flavor sector.

A. Saddle point: No external potential

Consider interacting NT electrons in the case of no external potential. Below we will imply, unless otherwise stated, that the Coulomb repulsion is large, so that the charge stiffness $K \gg 1$ [K defined in Eq. (46)]. At half filling, this system is described by the Lagrangian (56) with $A = 0$ and $\mu = 0$.

By raising the chemical potential above the gap one creates a charged excitation. Below we will describe such an excitation in detail following the approach of Levitov and Tsvelik.

As it has been shown in Ref. 13, the lowest energy charged excitation in this case is a combination of solitons of the charge and flavor modes characterized by the presence of the two length scales: flavor l_{fl} and charge $l_{\text{ch}} \sim K^{1/2}l_{\text{fl}}$, so that $l_{\text{ch}} \gg l_{\text{fl}}$. In such an excitation the soft flavor modes θ^a optimize the effective potential for the stiff charge mode θ^0 . This has been demonstrated in Ref. 13 by an example of adding an electron of a particular flavor, say, $\alpha = 1$, to the half-filled nanotube. In this case the field Θ_1 is changed by π and the other fields $\Theta_{2,3,4}$ are unchanged. According to the transformation (51), in such a configuration all the fields θ^0, θ^a change by $\pi/2$. Since $l_{\text{ch}} \gg l_{\text{fl}}$ in the limit of the large stiffness $K \gg 1$, solitons of the flavor modes θ^a can be viewed as infinitely sharp steps on the scale of l_{ch} . As suggested in Ref. 13, such a sharp “switching” of the flavor modes can optimize the potential term \mathcal{L}_{bs} in the total Lagrangian (56) by providing an effective potential $\propto g\bar{\mathcal{F}}_{\text{cl}}(\theta^0)$ for a

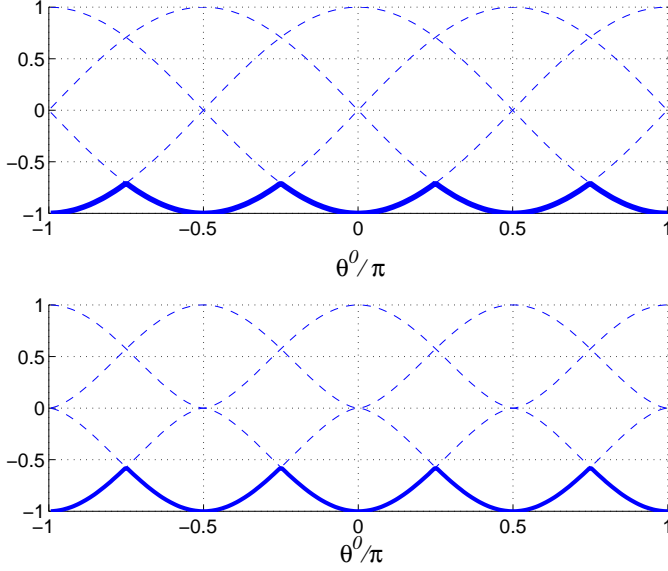


FIG. 3: Classical $\bar{\mathcal{F}}_{\text{cl}}(\theta^0)$ (top) and renormalized $\bar{\mathcal{F}}(\theta^0)$ (bottom) effective potentials (shown in bold) for the charge mode in the case of $K \gg 1$, Eqs. (60) and (63)

soliton of the stiff charge mode, where g is the renormalized value for the backscattering (45), and the function

$$\bar{\mathcal{F}}_{\text{cl}}(\theta^0) = \min_{\{\theta^a\}} \mathcal{F}(\theta^a, \theta^0) = \min \{\cos \theta^0, \sin \theta^0\} \quad (60)$$

is shown in the top panel of Fig. 3. For that the flavor modes θ^a should switch at the point when θ^0 is changed by $\pi/4$, in which case the *classical* soliton of the charge mode is of the form¹³

$$\theta_{\text{cl}}^0(x) = \begin{cases} 2 \cos^{-1} \tanh(u - x/l_{\text{ch}}), & x < 0, \\ \frac{\pi}{2} - 2 \cos^{-1} \tanh(u + x/l_{\text{ch}}), & x > 0, \end{cases} \quad (61)$$

where $l_{\text{ch}} = (K/g)^{1/2}$ and $\tanh u = \cos \pi/8$. Summarizing, according to Ref. 13, the lowest energy charge excitation corresponds to a *composite* soliton configuration in which the flavor solitons adjust themselves to provide effective potential for the stiff charge mode, such that the flavor of a resulting composite soliton Θ_α is confined to the region of size l_{fl} inside the charge soliton width $l_{\text{ch}} \gg l_{\text{fl}}$.

Authors of Ref. 13 have included effects of quantum fluctuations of the soft neutral sector in the scaling of the coupling g . However, in the adiabatic approximation $l_{\text{ch}} \gg l_{\text{fl}}$, the potential (60) is slow on the scale $a < l < l_{\text{fl}}$ on which quantum fluctuations of the fields θ^a are significant. Therefore, as it will be shown below in Sec. VI E, renormalization group treatment of the flavor modes results in the universal scaling dimension

$$\gamma = 8/5 \quad (62)$$

of the potential term (60).³⁹ As a result, the effective potential for the charge sector is

$$V_{\text{charge}} = g \bar{\mathcal{F}}(\theta^0), \quad \bar{\mathcal{F}}(\theta^0) = -(-\bar{\mathcal{F}}_{\text{cl}}(\theta^0))^\gamma, \quad (63)$$

where the renormalized backscattering amplitude

$$g \simeq \frac{1}{a^2} \left(\frac{\Delta_0}{D} \right)^\gamma \quad (64)$$

and the cutoff D is defined in Eq. (9). The function $\bar{\mathcal{F}}(\theta^0)$ is plotted in the lower panel of Fig. 3.

It can be shown⁴⁰ that the difference between the potentials (63) and (60) is qualitatively unimportant for the further discussion. It brings about only a numerical factor (order unity) for the charge soliton energy. Indeed, although the exact analytic form for the charge mode soliton with the potential term (63) is unavailable, it is qualitatively similar to the soliton (61) of Levitov and Tsvelik. Approximating the potential (63) by the piecewise-quadratic function, the charge mode soliton is

$$\theta_{\text{quad.}}^0(x) = \begin{cases} \frac{\pi}{4} e^{x/l_{\text{ch}}}, & x < 0, \\ \frac{\pi}{2} - \frac{\pi}{4} e^{-x/l_{\text{ch}}}, & x > 0, \end{cases} \quad (65)$$

with a charge soliton size

$$l_{\text{ch}} = \left(\frac{K}{2\gamma g} \right)^{1/2} \quad (66)$$

that is rescaled by a factor ≈ 1.26 compared to that in Eq. (61).

The important message of this subsection is that in the presence of the Coulomb repulsion the soft neutral modes adjust themselves in a saddle-point fashion to provide an effective potential (63) for the stiff charge mode. This effective potential has a period $\pi/2$ that is four times smaller than that for the backscattering potential (58) with *fixed* θ^a . Indeed, the lowest harmonic in the Fourier series

$$\bar{\mathcal{F}}(\theta^0) = \text{const.} + \sum_{n=1}^{\infty} f_n \cos(4n\theta^0) \quad (67)$$

is $\cos 4\theta^0$. The purpose of this period reduction is to lower the Coulomb energy by splitting the $\theta^0 \rightarrow \theta^0 + 2\pi$ charge excitation that carries four fermions [according to Eq. (52)] into four subsequent excitations each carrying a single fermion.

Going one step further, for the purposes of studying the crossover into the Wigner crystal regime where the charge sector dominates, one can make the following approximation that will be utilized below. Namely, one simplifies the effective potential for the charge sector by substituting the function $\bar{\mathcal{F}}(\theta^0)$ with its lowest harmonic from the series (67),

$$\bar{\mathcal{F}}(\theta^0) \approx f_1^* \cos 4\theta^0 \quad (68)$$

with the coefficient $f_1^* = \mathcal{O}(1)$ chosen in such a way that the energy of the charge soliton for the true potential (63) is equal to that for the potential (68). In this case the charge soliton takes the approximate form

$$\theta_{\text{approx}}^0(x) = \frac{1}{2} \cos^{-1} \tanh(-x/l_{\text{ch}}') \quad (69)$$

with the rescaled size $l_{\text{ch}}' = \frac{1}{4}(K/f_1^*g)^{1/2} \propto l_{\text{ch}}$.

Consider now the case of a finite fermion density corresponding to the chemical potential μ above the (renormalized) charge gap Δ . The ground state is then a lattice of composite solitons described above. In the case of small particle density, when the overlap of flavor soliton cores is exponentially small, such a configuration is a semi-classical one-dimensional Wigner crystal. Composite soliton centers correspond to classical positions of the electrons, and the exchange effects due to overlap between flavor solitons are negligible. Coulomb interaction (described by overlap of the charge solitons) maintains quasi-long range order in a finite system. In a real system the Coulomb repulsion is never infinitely long range, it is cut off at some screening length l_s (e.g. tube length or the distance to the metallic gate). The length l_s sets the scale for the charge stiffness $K = K_{qls \simeq 1}$.

In the Wigner crystal, charge states are compressible, with the density following the chemical potential in a continuous fashion. The compressibility of this system has been found in Ref. 13.

Raising the chemical potential one increases the particle density ρ . At some point the flavor soliton cores begin to overlap and exchange effects become important. At large density $\rho l_{\text{fl}} \gg 1$ the system enters the regime of the scale-invariant Tomonaga-Luttinger liquid. In this case the chemical potential is much greater than the Dirac gap, so that the electronic dispersion is approximately linear, corresponding to delocalized charge excitations. Since there is no phase transition in one dimension, the transition between the Wigner crystal and the Tomonaga-Luttinger liquid occurs smoothly, in a crossover fashion, as described above.

B. Incompressible states of classical bose fields

In the previous subsection we described the ground state of a stand-alone nanotube. Now let us add the external periodic potential (11).

In Section II the general argument was made about the ability of the external potential to lock the NT electron system into incompressible states in the presence of backscattering (45). Let us illustrate this point by the following example. Consider for simplicity a *classical* ground state of the Hamiltonian (44) for the fractional case of $m = 1/2$, corresponding to the chemical potential $\tilde{\mu} = 1/4$ [cf. Eq. (50)]. This is a configuration in which the solitons of the fields Θ_α occupy every other potential minimum, as shown in Fig. 4. This Figure is a result of a numerical minimization of the classical Hamiltonian (44) with respect to the fields Θ_α . For any rational density $m = p/q$ the period of each field Θ_α is $q\lambda_{\text{ext}}$, with $q = 2$ in Fig. 4. The *total* density $m_{\text{tot}} = 2$ is integer, hence the charge density period coincides with that of $U(x)$. In the absence of $U(x)$, all the Θ_α solitons would be equally separated from each other due to the Coulomb repulsion. The finite U configuration shown in Fig. 4 is a result of

an interplay between the mutually repelling solitons and a confining periodic potential. Fermionic exchange of the original problem (13) is manifest in the fact that solitons of the same flavor are located in different potential minima.

In what follows we will find the energy cost of a charged excitation in *quantum-mechanical* analogs of the commensurate classical soliton states. For that we will need to develop the analytical method that generalizes the phase soliton approach³² to the case of four modes and is able to take into account quantum fluctuations.

C. Phase soliton approach

Let us now outline the way to analytically study the ground state and excitation gaps for the commensurate states characterized by the density (1) in which m can be either integer or a simple fraction $m = p/q$. Following the standard prescription³² one starts from the bosonized Lagrangian (56) with the chemical potential corresponding to the density m according to Eq. (50), expands the bose-fields in powers of backscattering g_0 as

$$\begin{aligned} \theta^0 &= \bar{\theta}^0 + \theta^{0(1)} + \dots + \theta^{0(n)} + \dots , \\ \theta^a &= \bar{\theta}^a + \theta^{a(1)} + \dots + \theta^{a(n)} + \dots , \\ \theta^{0(n)} &= \mathcal{O}(g_0^n), \quad \theta^{a(n)} = \mathcal{O}(g_0^n), \end{aligned} \quad (70)$$

and then finds the effective Lagrangian

$$\mathcal{L}_m[\bar{\theta}^0, \bar{\theta}^a] = \mathcal{L}_0[\bar{\theta}^0, \bar{\theta}^a] + \mathcal{L}_m^{\text{int}}[\bar{\theta}^0, \bar{\theta}^a] \quad (71)$$

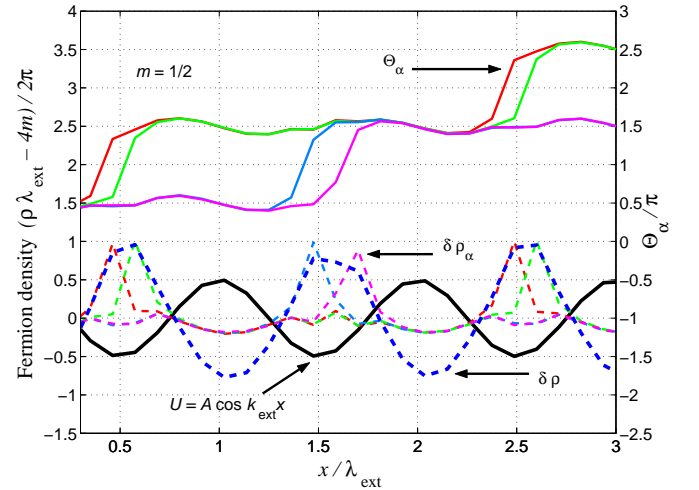


FIG. 4: Classical ground state of the Hamiltonian (44) for the fractional density $m = 1/2$. Solitons of the fields Θ_α (solid lines) as a result of numerical minimization of Eq. (44) for $\tilde{\mu} = 1/4$, $K = 10$, $g_0 = 48k_{\text{ext}}^2$, $A = K\epsilon_0$. Dashed lines are the corresponding partial flavor densities $\delta\rho_\alpha = \rho_\alpha - m/\lambda_{\text{ext}}$ counted from their average m/λ_{ext} . Bold dashed line is the total charge density counted from the total average $4m/\lambda_{\text{ext}}$. Note the period doubling for the fields $\Theta_\alpha(x)$.

for the phase modes $\bar{\theta}^0$ and $\bar{\theta}^a$ to the lowest order in g_0 . Here the first term is the Gaussian Lagrangian (57) as a function of the slow phase modes, and the potential energy $\mathcal{L}_m^{\text{int}}$ is of the order g_0^q (before integrating over quantum fluctuations).

From the Lagrangian $\mathcal{L}_m[\bar{\theta}^0, \bar{\theta}^a]$ one finds the commensurate ground state in which the phase modes $\bar{\theta}^0$ and $\bar{\theta}^a$ are constant. An excitation over such a ground state is a composite soliton of the slow phase modes $\bar{\theta}^0(x), \bar{\theta}^a(x)$. This composite soliton can be found as a saddle point of the Lagrangian $\mathcal{L}_m[\bar{\theta}^0, \bar{\theta}^a]$ in a way similar to that described above in Sec. VI A.

The charged phase mode Hamiltonian (4) can be obtained from the Lagrangian $\mathcal{L}_m[\bar{\theta}^0, \bar{\theta}^a]$ in two steps. First, one needs to find a saddle point of $\mathcal{L}_m[\bar{\theta}^0, \bar{\theta}^a]$ that describes a charged excitation of the lowest possible energy by adjusting the dynamics of the soft modes, in analogy to the procedure described above in Sec. VI A. We address this issue in the next subsection. Second, one needs to integrate out quantum fluctuations over the chosen saddle point to obtain the renormalized coupling g_m^* entering the charged phase mode Hamiltonian (4). We will briefly describe this procedure in Sec. VI E below.

The charge excitation gap then follows from the Hamiltonian (4), $\Delta_m \propto (Kg_m^*)^{1/2} \sim \Delta_{\text{ch}}$. The flavor sector of the Lagrangian $\mathcal{L}_m[\bar{\theta}^0, \bar{\theta}^a]$ freezes at the energy scale $\Delta_{\text{fl}} \sim K^{-1/2} \Delta_{\text{ch}}$ well below the flavor scale when $K \gg 1$. The resulting flavor Lagrangian $\mathcal{L}_m[\theta^0 = \bar{\theta}^0, \theta^a]$ describes excitations of the effective SU(4) “flavor” chain whose ground state in general has a gap $\sim \Delta_{\text{fl}}$.

D. Weak vs. strong coupling

Below we will demonstrate that the NT electron system has two qualitatively different regimes of coupling to external potential that are determined by a choice of the saddle point of the Lagrangian $\mathcal{L}_m[\bar{\theta}^0, \bar{\theta}^a]$. To illustrate this point, we consider the simplest phase mode Lagrangian, namely the one for the *integer* density m , in which case the decomposition (70) is trivial since it contains just one term for each mode. Hence $\mathcal{L}_m[\bar{\theta}^0, \bar{\theta}^a]$ is precisely the Lagrangian (56) written as a function of $\theta^{0,a} = \bar{\theta}^{0,a}$ with the chemical potential $\tilde{\mu}$ given by Eq. (50). [This integer- m case is also considered in detail in Sec. VII A below.]

The physical reason of having two regimes of coupling is that the behavior of the NT electrons is different depending on whether the fermions of the *same* flavor “feel” each other, i.e. their flavor soliton tails overlap (weak coupling), or they are far apart (strong coupling).

To define the regimes of coupling we need the size l_{fl} of the phase soliton $\bar{\theta}^a(x)$ of the flavor sector (“flavor scale”). For now we assume that l_{fl} is known. The scale l_{fl} will be obtained self-consistently as a result of integrating over quantum *fluctuations* (as outlined in Sec. VI E below and performed for particular densities in Sections VII and VIII).

Weak coupling

Consider the system’s ground state, *i.e.* the regular train of composite solitons described above, that corresponds to a particular density m . In the weak coupling regime the flavor soliton tails that correspond to fermions of the *same* flavor overlap. Physically, it means that the system “knows” that it is composed of the particles of different flavor since the role of exchange is important. An extreme example of this regime is a non-interacting system in which fermions of the same flavor effectively *repel* due to the Pauli principle, whereas fermions of different flavors do not notice each other.

Technically, the weak coupling regime is characterized by the *slow* “switching” of the flavor modes θ^a (described in Sec. VI A above) on the scale on which the phase of the *charge* part of the potential energy $\mathcal{L}_m^{\text{int}}[\bar{\theta}^0, \bar{\theta}^a]$ in the Lagrangian (71) changes by 2π . In our example of integer m , the potential energy is just the backscattering term (58) written as a function of the slow modes $\bar{\theta}^0, \bar{\theta}^a$. In this particular case we demand

$$\begin{aligned} mk_{\text{ext}}l_{\text{fl}} &\gg 2\pi, \\ 2\tilde{A}\sin k_{\text{ext}}l_{\text{fl}} &\gg 2\pi. \end{aligned} \quad (72)$$

The first condition in Eq. (72) requires the flavor excitation to be delocalized on the scale of separation $4\rho^{-1} = \lambda_{\text{ext}}/m$ between fermions of the same kind. It is equivalent to Eq. (2). The meaning of the second condition will be made more clear below. Practically, Eq. (72) is equivalent to (2) when the potential amplitude is not large, $A < K\hbar v/l_{\text{fl}}$. The weak coupling limit (72) results in the following approximation of the potential energy (58)

$$\begin{aligned} \mathcal{F}(\bar{\theta}^0 + mk_{\text{ext}}x - 2\tilde{A}\sin k_{\text{ext}}x, \bar{\theta}^a) \\ \approx J_m(2\tilde{A})\mathcal{F}(\bar{\theta}^0, \bar{\theta}^a) \rightarrow J_m(2\tilde{A})\bar{\mathcal{F}}_{\text{cl}}(\bar{\theta}^0). \end{aligned} \quad (73)$$

Here we have used the decomposition (29), discarded spatially oscillating terms (in other words, averaged \mathcal{F} over the period λ_{ext}), and denoted by the arrow the soft mode “switching” that produced the “optimized” potential (60). The procedure (73) as written is allowed for integer density m . In the case when the density $m = p/q$ is a simple fraction one needs to utilize the phase soliton approach to find the effective potential of order g_0^q and then perform a procedure analogous to Eq. (73).

The weak coupling limit is considered in detail in Sec. VII A for integer m and in Sec. VII B for the simplest fractional density $m = 1/2$.

Strong coupling

In the opposite limit (3) of strong coupling, overlap of the flavor solitons is small and hence exchange effects are insignificant. In this regime the system of four fermion flavors effectively behaves as a single-flavored system with

the total density (1). Physically this happens since when electron wavefunctions (represented by solitons) are *localized*, Coulomb interaction dominates exchange.

Technically, in our integer- m example, in the strong coupling limit

$$\begin{aligned} mk_{\text{ext}}l_{\text{fl}} &< 2\pi, \\ 2\tilde{A} \sin k_{\text{ext}}l_{\text{fl}} &< 2\pi. \end{aligned} \quad (74)$$

Now the soft mode “switching” (denoted by the arrow below) occurs *before* averaging over the period of the potential,

$$\begin{aligned} & \mathcal{F}(\bar{\theta}^0 + mk_{\text{ext}}x - 2\tilde{A} \sin k_{\text{ext}}x, \bar{\theta}^a) \\ & \rightarrow \bar{\mathcal{F}}(\bar{\theta}^0 + mk_{\text{ext}}x - 2\tilde{A} \sin k_{\text{ext}}x) \\ & = f_1 \cos(4\bar{\theta}^0 + m_{\text{tot}}k_{\text{ext}}x - 8\tilde{A} \sin k_{\text{ext}}x) \quad (75) \\ & + f_2 \cos(8\bar{\theta}^0 + 2m_{\text{tot}}k_{\text{ext}}x - 16\tilde{A} \sin k_{\text{ext}}x) + \dots \\ & \approx f_1^* \cos(4\bar{\theta}^0 + m_{\text{tot}}k_{\text{ext}}x - 8\tilde{A} \sin k_{\text{ext}}x). \end{aligned}$$

Here the Fourier coefficients f_n are defined in Eq. (67), and in the last line we used the approximation (68). Note dependence of the resulting potential energy on the *total density* $m_{\text{tot}} = 4m$.

In Section VIII we will study the effective potential obtained in Eq. (75) in detail. We will show that after the neutral fields $\bar{\theta}^a$ are integrated out, the resulting Lagrangian for the charge mode can be re-fermionized. The resulting Lagrangian will describe a *single* fermionic mode with the total density (1) and renormalized backscattering, that interacts with the external periodic potential. We will show that this procedure yields a semi-classical limit of finding charge excitations in the problem (56).

Now let us clarify the meaning of the second condition in Eqs. (72) and (74). Increasing the potential amplitude A beyond $K\hbar v/l_{\text{fl}}$ makes the external potential alter the flavor correlations that develop on the scale l_{fl} . This can draw the system into the weak coupling limit (72). This situation is similar to the non-interacting case considered in Section IV above. In both cases, a very strong potential amplitude averages out the effect of the external potential.

E. Effect of quantum fluctuations

Finally, let us briefly outline the way to take into account quantum fluctuations over the chosen saddle point. For simplicity here we will mostly focus on the limit $K \gg 1$ of strong electron interactions, in which case fluctuations of the charge mode can be to the lowest order discarded.

As an example we will renormalize the charge gap Δ for the case of a half-filled nanotube in the absence of external potential. The saddle point for this case was described in Sec. VIA above. Quantum fluctuations of

the neutral modes are described by the Lagrangian of the form [cf. Eq. (56)]

$$\begin{aligned} \mathcal{L}[\theta^a] &= \frac{\hbar v}{2\pi} \int dx \sum_{a=1}^3 \left(\frac{1}{v^2} (\partial_t \theta^a)^2 - (\partial_x \theta^a)^2 \right) \\ &\quad - \hbar v \int dx \tilde{g} \prod_{a=1}^3 \cos \theta^a + (\cos \leftrightarrow \sin), \end{aligned} \quad (76)$$

where $\tilde{g} = (g_0/\pi) \cos \theta^0$ and g_0 is proportional to the bare NT gap Δ_0 [Eq. (45)]. Adiabaticity of the charged mode at $K \gg 1$ ensures that $\tilde{g} \simeq \text{const.}$ on the length scales $a < l < l_{\text{fl}}$ where quantum fluctuations of the flavor modes are relevant. With each neutral field in the product in Eq. (76) contributing to the scaling dimension by $1/4$, flavor fluctuations result in the net scaling dimension

$$\gamma_0 = \frac{3}{4} \quad (77)$$

for the potential term in Eq. (76), yielding the scaling law

$$\tilde{g}(l) = \tilde{g}(a) \left(\frac{l}{a} \right)^{-\gamma_0}, \quad (78)$$

where l is the renormalization group scale and a is the tube radius. Since $\gamma_0 < 2$ the coupling \tilde{g} is relevant and grows (compared to the kinetic term). The renormalization group flow (78) *stops* on the scale $l = l_{\text{fl}}$ on which the potential energy becomes comparable to the kinetic energy of the flavor sector, since the perturbative renormalization group works only while the *renormalized* coupling $\tilde{g}(l)$ stays small.⁴¹ For the larger scales $l > l_{\text{fl}}$ the potential energy dominates and the problem becomes classical.

The scale l_{fl} has a two-fold meaning.

First, it is the *correlation length* for the flavor modes. It can be estimated self-consistently from the balance of kinetic and potential terms

$$\tilde{g}(l_{\text{fl}}) \simeq \frac{1}{l_{\text{fl}}^2}. \quad (79)$$

Beyond $x \simeq l_{\text{fl}}$ the correlation functions of the θ^a fields decay exponentially (rather than in a power-law fashion).

From Eqs. (78) and (79) we obtain the renormalized potential (63) for the charge mode with the renormalized backscattering (64) and the scaling dimension (62),

$$\gamma = \frac{2}{2 - \gamma_0}. \quad (80)$$

The second meaning of the scale l_{fl} is the *size of the flavor soliton*. Indeed, Eq. (79) is exactly the way to estimate the soliton size of the fields θ^a in a classical sine-Gordon model [Eq. (76) with renormalized coupling $\tilde{g} = \tilde{g}(l_{\text{fl}})$].

Since the charge sector is stiff, the excitation gap Δ is dominated by the charge soliton energy. The latter

can be now estimated classically from the effective charge mode Lagrangian

$$\begin{aligned}\mathcal{L}_{\text{charge}} &= \frac{\hbar v}{\pi} \int dx \left(\frac{1}{2v^2} (\partial_t \theta^0)^2 - \frac{K}{2} (\partial_x \theta^0)^2 - V_{\text{charge}} \right) \\ &\approx \frac{\hbar v}{\pi} \int dx \left(\frac{1}{2v^2} (\partial_t \theta^0)^2 - \frac{K}{2} (\partial_x \theta^0)^2 - g f_1^* \cos 4\theta^0 \right) \end{aligned}\quad (81)$$

where we used the saddle point approximation (63), (64) and (68) outlined in Sec. VI A above. The effective Lagrangian (81) yields the gap^{13,24}

$$\Delta \simeq K^{1/2} D^{1/5} \Delta_0^{4/5}. \quad (82)$$

The renormalization group approach can be further utilized to include corrections due to finite charge stiffness K . In this case the scaling of the excitation gap acquires corrections of the order of

$$\eta = \frac{1}{\sqrt{K}}. \quad (83)$$

The approach that self-consistently includes interplay between the charge and flavor soliton scales yields⁴⁰

$$\Delta \simeq K^{\frac{1}{2}-\alpha} D^{\frac{1-\eta}{5-\eta}} \Delta_0^{\frac{4}{5-\eta}}, \quad \alpha = \frac{\eta}{10-2\eta}. \quad (84)$$

The latter expression is valid also for the noninteracting case $K = 1$, $\Delta = \Delta_0$.⁴²

The same approach applies to estimating the excitation gap for the commensurate ground state in the presence of the external potential $U(x)$. This gap is the (renormalized) energy of the phase soliton. As in the previous case, fluctuations of the flavor sector will result in a certain scaling dimension γ_m for the effective potential in the phase mode Lagrangian $\mathcal{L}_m[\bar{\theta}^0, \bar{\theta}^a]$ introduced in Sec. VI C above. This will yield the renormalization group flow

$$g_m(l) = g_m(a) \left(\frac{l}{a} \right)^{-\gamma_m} \quad (85)$$

for the corresponding coupling g_m in the effective potential of the charge sector. As it will be demonstrated below in Sections VII and VIII, the exponent γ_m will depend on the density (1) as well as whether the system is in the weak or in the strong coupling limit (defined in Sec. VID).

Analogously, in the case of the phase soliton excitation, the fluctuations of the flavor sector will be relevant if $\gamma_m < 2$. In this case the potential energy in the Lagrangian $\mathcal{L}_m[\bar{\theta}^0, \bar{\theta}^a]$ will grow. The renormalization group flow will stop as soon as the scale reaches the correlation radius l_{fl} that can be estimated self-consistently,

$$g_m(l_{\text{fl}}) \simeq \frac{1}{l_{\text{fl}}^2}. \quad (86)$$

From the latter condition one obtains the flavor scale l_{fl} and the renormalized value $g_m^* \equiv g_m(l_{\text{fl}})$ of the coupling

with its scaling dimension

$$\tilde{\gamma}_m = \frac{2}{2 - \gamma_m} \quad (87)$$

[modulo corrections $\mathcal{O}(\eta)$] that can then be used in the effective classical Hamiltonian (4) to estimate the corresponding excitation gap.

VII. WEAK COUPLING LIMIT

In the present Section we will estimate excitation gaps in the weak coupling limit introduced in Sec. VID. We will specifically focus on the two cases. In Sec. VII A we consider the simplest case of *integer* density m studied in Ref. 24. In Sec. VII B we consider the simplest *fractional* state $m = 1/2$.

Our course of action has been outlined in Section VI above. Technically, it will be more convenient to first work in the basis of the original fields Θ_α and later utilize the transformation (51) to obtain the Lagrangian $\mathcal{L}_m[\bar{\theta}^0, \bar{\theta}^a]$ in the charge-flavor basis. First we will find the classical ground state of the Hamiltonian \mathcal{H}'_{cl} [Eq. (48)] by decomposing the fields $\Theta_\alpha(x)$ in a series in the coupling g_0 ,

$$\Theta_\alpha = \bar{\Theta}_\alpha + \Theta_\alpha^{(1)} + \dots, \quad \Theta_\alpha^{(n)} = \mathcal{O}(g_0^n). \quad (88)$$

We will derive the effective potential $V_m[\bar{\Theta}_\alpha]$ for the “slow” phase modes $\bar{\Theta}_\alpha$ that are constant in the commensurate state with density m . Next we will obtain the phase mode Lagrangian $\mathcal{L}_m[\bar{\theta}^0, \bar{\theta}^a]$ by applying the canonical transformation (51) and adding the Gaussian kinetic energy (57) for the phase modes. To find the charge phase mode Hamiltonian (4) we will integrate out the fluctuations of the soft flavor fields $\bar{\theta}^a$ using the Lagrangian $\mathcal{L}_m[\bar{\theta}^0, \bar{\theta}^a]$ as described above. Finally, we will estimate the charge excitation energy as that of the phase soliton of the stiff charged phase mode governed by the Hamiltonian of the form (4).

A. Integer density

In the present subsection we find excitation gaps for the integer density m . Our treatment covers the results announced in Ref. 24. The integer- m case is trivial in a sense that it is enough to keep the first term in the expansion (88).

Below we find a classical ground state of the Hamiltonian (48) with the chemical potential $\tilde{\mu}$ given by Eq. (50). For that we need to solve the Euler-Lagrange equations

$$\frac{\delta \mathcal{H}'_{\text{cl}}}{\delta \Theta_\alpha} = 0 \quad (89)$$

perturbatively in g_0 . Using the decomposition (88), in the lowest order in g_0 we find the effective potential for

the “slow” components

$$V_m[\bar{\Theta}_\alpha] = \frac{\hbar v}{4\pi} \int dx g_0 J_m(2\tilde{A}) \sum_\alpha \cos 2\bar{\Theta}_\alpha. \quad (90)$$

From the potential (90) it follows that the ground state is non-degenerate, with the fields $\bar{\Theta}_\alpha$ being all *equal* and *constant*. Their ground state values are either $\pi/2$ or 0 depending on the sign of the Bessel function. Such a state for $m = 1$ is schematically shown in Fig. 1(d).

Adding the kinetic energy (57) and using the canonical transformation (51) we obtain the phase mode Lagrangian (71) with the potential term

$$\begin{aligned} -\mathcal{L}_m^{\text{int}} &= \frac{\hbar v}{\pi} \int dx g_0 J_m(2\tilde{A}) \mathcal{F}(\bar{\theta}^0, \bar{\theta}^a) \\ &\rightarrow \frac{\hbar v}{\pi} \int dx g_m \cos 4\bar{\theta}^0. \end{aligned} \quad (91)$$

Here we denoted the saddle point optimization (“switching”) of the flavor fields by an arrow according to Eq. (73) and kept the lowest harmonic for the potential (67) [utilizing the approximation (68)] to obtain the effective charge mode coupling

$$g_m = g_0 f_1^* J_m(2\tilde{A}). \quad (92)$$

Integration over the Gaussian fluctuations of the neutral phase fields $\bar{\theta}^a$ is made in accord with Sec. VI E. We obtain the scaling law (85) with²⁴

$$\gamma_m = 3/4, \quad m = 0, \pm 1, \pm 2, \dots \quad (93)$$

for the coupling (92) when $K \gg 1$. As in the case of a stand-alone nanotube (Sec. VI E above), quantum fluctuations of each of the three flavor modes θ^a contribute by $1/4$ to the scaling dimension of g_m .

From the self-consistency condition (86) we obtain the flavor soliton size

$$l_{\text{fl}} \sim a \left(\frac{D}{\Delta_m^{(0)}(\tilde{A})} \right)^{4/5}. \quad (94)$$

Here the 1D bandwidth D is defined in Eq. (9), and the “bare” minigaps

$$\Delta_m^{(0)}(\tilde{A}) = \Delta_0 |J_m(2\tilde{A})| \quad (95)$$

are given by their noninteracting values (30) with the screened potential amplitude \tilde{A} defined in Eq. (49).

Finally, the renormalized minigap Δ_m can be estimated as energy of the *classical* charge soliton from the effective Hamiltonian that follows from (91)

$$\mathcal{H}_m[\bar{\theta}^0] = \frac{\hbar v}{\pi} \int dx \left\{ \frac{K}{2} (\partial_x \bar{\theta}^0)^2 + g_m^* \cos 4\bar{\theta}^0 \right\}. \quad (96)$$

The Hamiltonian (96) is of the form (4) with

$$g_m^* \simeq \frac{1}{l_{\text{fl}}^2}. \quad (97)$$

From the Hamiltonian (96) we find the charge soliton size

$$l_{\text{ch}} \simeq K^{1/2} l_{\text{fl}}. \quad (98)$$

The corresponding charge soliton energy gives an estimate for a renormalized minigap value²⁴

$$\Delta_m \simeq K^{1/2} D^{1/5} \left(\Delta_m^{(0)}(\tilde{A}) \right)^{4/5}. \quad (99)$$

Incorporating quantum fluctuations of the charge sector one can obtain the $\mathcal{O}(\eta)$ corrections to the exponents in Eq. (99) that are the same as in Eq. (84).⁴⁰

As noted in Ref.²⁴, the qualitative features of the non-interacting minigaps (30) persist in the interacting case. Namely, as a function of the *screened* potential amplitude (49), the minigaps (99) oscillate, collapsing to zero at particular values of \tilde{A} . However, minigaps (99) are strongly *enhanced* in magnitude compared to (30) due to electron interactions. Also the dependence of the minigaps on both the bare backscattering Δ_0 and on the periodic potential amplitude A has a characteristic power law behavior which, in the limit of strong interactions $K \gg 1$, is given by a universal power law $4/5$. This power law is a manifestation of the SU(4) flavor symmetry in the nanotube near half filling.

What is the cost of adding electron’s *flavor* on top of its charge? The answer comes from the phase mode Lagrangian (71) with the potential term (91). This Lagrangian is formally equivalent (up to the substitution $g_m \leftrightarrow g$) to the problem (56) in the absence of the external potential. The issue of effective flavor dynamics in the latter case has been addressed by Levitov and Tsvelik. They have shown that, on the energy scale below Δ_{ch} of the frozen charge sector, the flavor sector is governed by the effective Gross–Neveu Lagrangian^{13,43}

$$\begin{aligned} \mathcal{L}_{\text{GN}} &= \frac{\hbar v}{\pi} \int dx \left\{ \frac{1}{2} (\partial_\mu \theta^a)^2 - g_{\text{GN}} \sum_{a>b} \cos 2\theta^a \cos 2\theta^b \right\} \\ &= \hbar v \int dx \{ i \bar{\chi}_j \gamma_\mu \partial_\mu \chi_j - g_{\text{GN}} (\bar{\chi}_j \chi_j) (\bar{\chi}_{j'} \chi_{j'}) \} \end{aligned} \quad (100)$$

where χ_j are the Majorana fermions and the Gross–Neveu coupling in our case is $g_{\text{GN}} \propto g_m$. The excitations of the model (100) are *massive* relativistic particles transforming according to different representations of the O(6) group.⁴⁴

B. Fractional density $m = 1/2$

So far in this work we considered incompressible states with an integer filling of m fermions per potential period. Such states arise due to a single electron diffraction on the periodic potential, and their spectrum is qualitatively similar in the interacting and non-interacting systems. However, as we will show in the present subsection, in the presence of Coulomb interactions ($K > 1$) additional

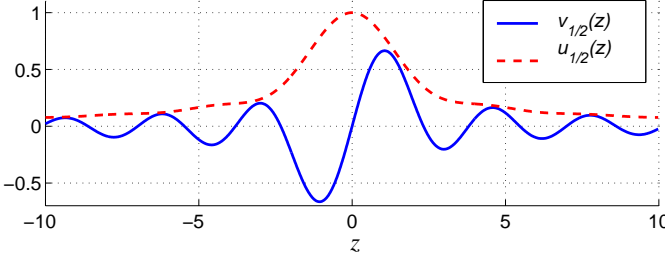


FIG. 5: The functions $v_{1/2}$ and $u_{1/2}$ defined in Eqs. (109) and (110). We find that $v_{1/2}(z) < u_{1/2}(z)$ holds for all z . Zeroes of $v_{1/2}$: $z = 0, \pm 2.33, \pm 3.80, \pm 5.47, \dots$.

incompressible states appear. This happens since in this case the restrictions due to the noninteracting Bloch theory are lifted, which leads to incompressible states with fractional fermion density m .

Below we consider the simplest nontrivial case of an interaction-induced state with a fractional density $m = 1/2$. Our course of action will be similar to the one utilized in Sec. VII A above. We start from finding a classical ground state of the Hamiltonian (48) for the commensurate state which is characterized by the chemical potential

$$\tilde{\mu} = \frac{1}{4} \quad (101)$$

in accord with Eq. (50).

The main difference with the integer- m case described above is that the average of the $\mathcal{O}(g_0)$ term in the potential energy over *two* successive potential periods is zero. To obtain the $\mathcal{O}(g_0^2)$ potential energy we include first *two* terms in the series (88).

Below we find the classical $m = 1/2$ soliton configuration perturbatively in backscattering g_0 by minimizing the energy (48). In analogy to Sec. VII A above, we look for an effective potential $V_{1/2}[\bar{\Theta}_\alpha]$ for the “slow” fields $\bar{\Theta}_\alpha$ defined in Eq. (88).

The Euler – Lagrange equations (89) for the Hamiltonian (48) yield

$$\Theta_\alpha^{(1)xx} + \frac{K-1}{4} S_{xx}^{(1)} = -\frac{g_0}{2} \sin \left(2\bar{\Theta}_\alpha + \frac{1}{2}k_{\text{ext}}x - 2\tilde{A} \sin k_{\text{ext}}x \right), \quad (102)$$

where $S = \sum \Theta_\alpha$. Integrating Eq. (102) we obtain

$$\Theta_\alpha^{(1)x} = \frac{1-K}{4} S_x^{(1)} + \frac{g_0}{k_{\text{ext}}} \tilde{\Theta}_\alpha, \quad (103)$$

$$S_x^{(1)} = \frac{g_0}{Kk_{\text{ext}}} \sum \tilde{\Theta}_\alpha, \quad (104)$$

$$\tilde{\Theta}_\alpha = \sum_m \frac{J_m(2\tilde{A})}{1-2m} \cos \left(2\bar{\Theta}_\alpha + \left(\frac{1}{2} - m \right) k_{\text{ext}}x \right) \quad (105)$$

Substituting Eqs. (103) and (105) into the Hamiltonian (48), after somewhat lengthy but straightforward algebra the slow mode potential follows:

$$V_{1/2} = \frac{\hbar v g'_0}{16\pi} \int dx \left\{ (4 - \kappa) v_{1/2}(2\tilde{A}) \sum_\alpha \cos 4\bar{\Theta}_\alpha + \kappa \sum_{\alpha \neq \alpha'} \left(u_{1/2}(2\tilde{A}) \cos(2\bar{\Theta}_\alpha - 2\bar{\Theta}_{\alpha'}) - v_{1/2}(2\tilde{A}) \cos(2\bar{\Theta}_\alpha + 2\bar{\Theta}_{\alpha'}) \right) \right\} \quad (106)$$

Here

$$g'_0 = \left(\frac{g_0}{k_{\text{ext}}} \right)^2 = \left(\frac{\Delta_0}{\epsilon_0 a} \right)^2, \quad (107)$$

$$\kappa = \frac{K-1}{K}, \quad (108)$$

and the functions $v_{1/2}$ and $u_{1/2}$ are defined as

$$v_{1/2}(z) = \sum_{m=-\infty}^{\infty} \frac{J_m(z) J_{1-m}(z)}{(2m-1)^2}, \quad (109)$$

$$u_{1/2}(z) = \sum_{m=-\infty}^{\infty} \left(\frac{J_m(z)}{1-2m} \right)^2 \quad (110)$$

with z being a shorthand for $2\tilde{A}$. The functions $v_{1/2}(z)$ and $u_{1/2}(z)$ are plotted in Fig. 5.

In the commensurate state we find that the minimum value

$$\min V_{1/2}[\bar{\Theta}_\alpha] = -\frac{\hbar v g'_0}{4\pi} \int dx \left\{ 4|v_{1/2}(2\tilde{A})| + \kappa u_{1/2}(2\tilde{A}) \right\} \quad (111)$$

of the potential (106) corresponds to the slow modes $\{\bar{\Theta}_\alpha\}$ being an arbitrary permutation of a set $\{\phi_1 \phi_1 \phi_2 \phi_2\}$, with $\phi_{1,2} = \pm\pi/4$ for $v_{1/2}(2\tilde{A}) > 0$ and $\phi_1 = 0, \phi_2 = \pi/2$ for $v_{1/2}(2\tilde{A}) < 0$.

Let us now discuss the symmetry of the obtained commensurate classical state. The ground state degeneracy in the noninteracting case ($\kappa = 0$) is equal to 2^4 . This follows from the potential (106) in which only the first term is nonzero. We find that in the presence of interactions ($\kappa > 0$), the other terms in (106) reduce this degeneracy from 16 to six. This result could have been foreseen without any calculation since the remaining degeneracy is just a number of configurations in which any two *differ*

ent fields, Θ_α and Θ_β with $\alpha \neq \beta$, are placed in the same minimum of the external potential. In other words, in the bosonized treatment the effect of fermionic *exchange* manifests itself in a stronger repulsion between the solitons of the same flavor. This is in agreement with the numerical minimization performed in Sec. VI B, Fig. 4. The symmetry of the obtained classical ground state is schematically illustrated in Fig. 1(e).

$$-\mathcal{L}_{1/2}^{\text{int}} = \frac{\hbar v g'_0}{4\pi} \int dx \left\{ (4 - \kappa) v_{1/2}(2\tilde{A}) \mathcal{F}(2\bar{\theta}^0, 2\bar{\theta}^a) - \kappa v_{1/2}(2\tilde{A}) \sum_a \cos 2\bar{\theta}^0 \cos 2\bar{\theta}^a + \kappa u_{1/2}(2\tilde{A}) \sum_{a>b} \cos 2\bar{\theta}^a \cos 2\bar{\theta}^b \right\}. \quad (113)$$

Here the function \mathcal{F} is defined in Eq. (55).

Let us discuss the potential energy (113). Its first term has scaling dimension 3 and is irrelevant. The second term of the potential (113) is responsible for the charge excitation gap Δ_{ch} . This term has scaling dimension

$$\gamma_{1/2} = 1 \quad (114)$$

and grows under the renormalization group flow. Finally, the third term is marginal. It describes the SU(4) *flavor* physics on the energy scale $\Delta_{\text{fl}} \sim K^{-1/2} \Delta_{\text{ch}}$.

It is notable that for certain potential amplitude values A^* such that $v_{1/2}(2\tilde{A}^*) = 0$, the second term of the potential (113) vanishes, and so does the charge excitation gap. This is analogous to the integer m case considered above, where the gaps (99) collapsed at the zeroes of the Bessel functions.

Now we proceed to finding the excitation gap. For generic potential amplitude values the effective potential for the charge mode can be derived by performing the saddle-point optimization of the second term of the potential (113) in a way similar to that described in Sec. VI A and VII A above. Adding an extra electron to the system (112) corresponds to a composite phase soliton in which the $\bar{\theta}^a$ fields “switch” by $\pi/2$ in the middle of a slow charged phase soliton, at the point when $\cos 2\bar{\theta}^0 = 0$. (It is possible to show⁴⁰ that although at this very point the effective sine-Gordon coupling $\propto \cos 2\bar{\theta}^0$ for the neutral sector vanishes, the flavor soliton has a finite size and energy. This is the case since away from the center of the charged soliton, $\cos 2\bar{\theta}^0 \neq 0$ giving the finite flavor scale.) Below we show that the adjustment of the neutral sector yields the effective potential

$$V_{\text{charge}}^{(1/2)}[\bar{\theta}^0] = g_{1/2}^* \bar{\mathcal{F}}^{(1/2)},$$

$$\bar{\mathcal{F}}^{(1/2)} = - \left| \bar{\mathcal{F}}_{\text{cl}}^{(1/2)} \right|^{\tilde{\gamma}_{1/2}} = - f_1^{*(1/2)} \cos 4\bar{\theta}^0 + \text{const.} \quad (115)$$

for the charge mode. Here the bare value of the coupling

$$g_{1/2} = \frac{1}{4} \kappa g'_0 \left| v_{1/2}(2\tilde{A}) \right|, \quad (116)$$

The effective phase mode Lagrangian

$$\mathcal{L}_{1/2}[\bar{\theta}^0, \bar{\theta}^a] = \mathcal{L}_0[\bar{\theta}^0, \bar{\theta}^a] + \mathcal{L}_{1/2}^{\text{int}}[\bar{\theta}^0, \bar{\theta}^a] \quad (112)$$

is given by the sum of the Gaussian part \mathcal{L}_0 [Eq. (57)] and the potential energy $-\mathcal{L}_{1/2}^{\text{int}} = V_{1/2}$ written in the charge-flavor basis (51):

the scaling dimension

$$\tilde{\gamma}_{1/2} = 2 \quad (117)$$

and the coefficient

$$f_1^{*(1/2)} = \frac{1}{2}. \quad (118)$$

Consider first the neutral sector adjustment at the classical level. The bare potential $\bar{\mathcal{F}}_{\text{cl}}^{(1/2)}$ originates from the saddle-point optimization (Fig. 6)

$$\sum_a \cos 2\bar{\theta}^0 \cos 2\bar{\theta}^a \rightarrow \bar{\mathcal{F}}_{\text{cl}}^{(1/2)}(\bar{\theta}^0) = - |\cos 2\bar{\theta}^0|. \quad (119)$$

Next we include effect of quantum fluctuations of the neutral sector. By integrating over fluctuations of the flavor fields $\bar{\theta}^a$ we obtain the flow (85) for the coupling $\propto g_{1/2} \cos 2\bar{\theta}^0$ with the scaling exponent (114). From the self-consistency relation (86) we find the flavor soliton scale

$$l_{\text{fl},1/2} \sim \frac{a}{\kappa |v_{1/2}(2\tilde{A})|} \left(\frac{\epsilon_0}{\Delta_0} \right)^2, \quad (120)$$

where a is the tube radius, the renormalized charge mode coupling

$$g_{1/2}^* \simeq \frac{1}{l_{\text{fl},1/2}^2}, \quad (121)$$

and, using Eq. (87), the scaling dimension (117) for the classical optimized potential (119).

Note that the value $f_1^{*(1/2)}$ in the present case is not approximate [as one could anticipate from the procedure leading to Eq. (68)], but *exact*. This is a result of the specific value of the scaling (114). The functions $\bar{\mathcal{F}}_{\text{cl}}^{(1/2)}$ and $\bar{\mathcal{F}}^{(1/2)}$ are shown in Fig. 6. They both have a period $\pi/2$ that corresponds to adding unit charge according to Eq. (52). The charge soliton in the present case has the *exact* form (69) with the correspondingly adjusted size l_{ch} .

Adding the potential (115) to the kinetic term we obtain the effective Hamiltonian of the form (4) for the charge mode:

$$\mathcal{H}_{1/2}[\bar{\theta}^0] \simeq \frac{\hbar v}{\pi} \int dx \left\{ \frac{K}{2} (\partial_x \bar{\theta}^0)^2 + g_{1/2}^* \cos 4\bar{\theta}^0 \right\}. \quad (122)$$

From the Hamiltonian (122) the renormalized minigap follows:

$$\Delta_{1/2} \simeq \frac{K-1}{\sqrt{K}} D |v_{1/2}(2\tilde{A})| \left(\frac{\Delta_0}{\epsilon_0} \right)^2. \quad (123)$$

Here the 1D band width D is defined in Eq. (9), and we neglected quantum fluctuations of the charge sector.

Let us pause to discuss the obtained excitation gap (123). We note that its renormalized value is strongly *enhanced* by the band width D [even more so than for the integer- m case of Sec. VII A] due to fluctuations of the flavor sector. We also note the $m = 1/2$ incompressible state is explicitly interaction-induced. Indeed, although the charge excitation gap $\Delta_{1/2}$ is derived in the strongly interacting limit $K \gg 1$, Eq. (123) gives a correct noninteracting limit $\Delta_{1/2} = 0$ that is expected from the single particle Bloch theory. Formally, when $K = 1$, *both* flavor and charge gaps are zero since the last two terms of the potential (113) vanish.

The weak coupling estimate (123) is valid when the flavor soliton size (120) is large,

$$l_{\text{fl},1/2} \gg \lambda_{\text{ext}}, \quad (124)$$

according to the condition (2) above. Practically, due to the large bandwidth D , Eq. (124) requires a very small

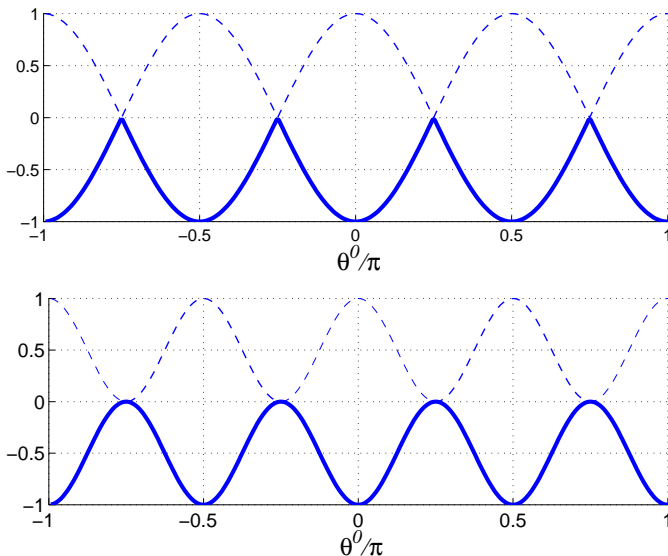


FIG. 6: Classical $\bar{\mathcal{F}}_{\text{cl}}^{(1/2)}(\theta^0)$ (top) and renormalized $\bar{\mathcal{F}}^{(1/2)}(\theta^0)$ (bottom) effective potentials (shown in bold) for the charge mode at density $m = 1/2$ in the case of $K \gg 1$, Eqs. (115) and (119)

bare gap Δ_0 . For typical values of parameters, $\lambda_{\text{ext}} \sim 0.1 \mu\text{m}$ and $\Delta_0 = 10 \text{ meV}$, the soliton scale defined in Eq. (120) is small compared to the potential period λ_{ext} , $l_{\text{fl},1/2} \sim 10 \text{ nm} < \lambda_{\text{ext}}$, and the condition (124) does not hold. In this case the excitation gap will be given by the strong coupling limit value $\bar{\Delta}_{1/2}$ obtained below in Section VIII.

However, even for the above mentioned parameter values there are cases when the result (123) is applicable. This happens when the flavor soliton size $l_{\text{fl},1/2}$ becomes large: either when one takes the tube that is almost metallic, $\Delta_0 \sim 1 \text{ meV}$, in which case $l_{\text{fl},1/2} \sim 1 \mu\text{m} > \lambda_{\text{ext}}$, or for near certain potential amplitude values A^* that correspond to zeroes of the function $v_{1/2}(2\tilde{A})$, as shown in Fig. 5.

In the special case when the potential amplitude $A = A^*$ is such that the coupling $g_{1/2}$ vanishes, $v_{1/2}(2\tilde{A}) = 0$, the charged excitation is *gapless*, but *the flavor sector remains gapped*. Its gap Δ_{fl} can be estimated from the effective $O(6) \simeq SU(4)$ Gross–Neveu Lagrangian of the form (100) that is given by the last term of the Lagrangian (113), where now the coupling $g_{\text{GN}} \propto u_{1/2}(2\tilde{A}^*) \neq 0$.

C. Summary

In the present Section we have considered the system in the limit (72) in which effects of *exchange* are important. The quantum-mechanical nature of the system is manifest in that the flavor excitation is delocalized over several potential periods.

As in the noninteracting case of weak coupling considered in Section IV, in this limit the properties of the system are dominated by the *kinetic energy*. Naturally, as shown in Sec. VII A, the excitation spectrum for *integer* densities is adiabatically connected to that of the noninteracting Dirac electrons (Section IV).

In Sec. VII B we have seen that electron interactions can play a greater role by opening minigaps at fractional densities. We have estimated such a minigap for the density $m = 1/2$ [Eq. (123)]. This minigap closes in the absense of the Coulomb repulsion as expected from the noninteracting Bloch theory.

Both integer and fractional- m minigaps appear to be *enhanced* both by the positive powers of bandwidth D and by the square root $K^{1/2}$ of the interaction strength.

We have also shown that the effective “flavor” dynamics on the background of the frozen charge sector is that of the $SU(4)$ spin chain with massive excitations. Namely, the flavor excitations both for the integer m and for $m = 1/2$ are governed by the $O(6) \simeq SU(4)$ Gross–Neveu Lagrangian (100) that possesses an excitation gap Δ_{fl} . Whereas in the former case the Gross–Neveu coupling vanishes with the charged gap, in the latter case of $m = 1/2$, the coupling g_{GN} is manifestly non-zero. Moreover, it is a function of the external potential and thus *can be externally controlled*. We note that the effective Gross–Neveu flavor physics originates due to the the

SU(4) invariance of the original problem (56) and (13) in the forward scattering approximation. This symmetry is present already at the “tree level” rather than arises in the course of renormalization.

It is also remarkable that the obtained flavor excitations are *massive* (gapped). They originate from paying the energy cost (of the order of exchange integral) of adding electron flavor to the system. One may contrast the massive SU(4) flavor excitations for the nanotube electrons with the case of the SU(2) invariant Hubbard model considered by Ogata and Shiba²⁵ for the spin- $\frac{1}{2}$ fermions. There, in the absence of the external potential in the limit of infinite on-site repulsion the charge sector freezes. Using the Bethe ansatz technique, Ogata and Shiba have shown that the effective spin- $\frac{1}{2}$ Hamiltonian in the latter case is that of the Heisenberg antiferromagnet with *gapless* excitations.

VIII. STRONG COUPLING LIMIT

The purpose of the present Section is to derive the effective Hamiltonian for strongly interacting nanotube electrons [Eq. (132) below] valid in the limit (74). In this regime the effects of fermionic exchange are unimportant since the flavor excitation scale l_{fl} is much smaller than the potential period, $l_{\text{fl}} \ll \lambda_{\text{ext}}$, and the overlap of the flavor cores of the composite solitons (considered in Sec. VI A) is exponentially suppressed. The dynamics in the strong coupling limit is determined primarily by

electron *interactions*. This regime can be thought of as a semi-classical description in which the electrostatics of the charge mode determines the nature of incompressible states and excitations.

Below we will show that in this case the system of NT electrons of the four flavors Θ_{α} effectively behaves as that of a single flavor Θ with the total density (1). We will obtain the effective Lagrangian $\mathcal{L}_{\text{eff}}[\Theta]$ that describes the dynamics of this mode. After re-fermionization that Lagrangian will correspond to the effective Hamiltonian (132) of *spinless* interacting Dirac fermions with renormalized gap Δ' [Eq. (135)] that are subjected to the external potential (11). At the end of this Section we will estimate charge gaps for the corresponding incompressible electron states, and in the following Section we will use this Hamiltonian to draw the phase diagram.

A. Lagrangian for the charged phase mode

In Sec. VI E above we have derived the approximate Lagrangian (81) describing the dynamics of the charge mode after integrating out quantum fluctuations of the flavor sector. The main result of that integration is that the flavor sector reduces the period of the effective charge mode potential by a factor of four, $\cos \theta^0 \rightarrow \cos 4\theta^0$, Eq. (68). Under the adiabaticity condition (74), the same saddle point treatment applies to the full system (56) in the presence of the external potential. In this case the effective charge mode Lagrangian is

$$\begin{aligned} \mathcal{L}_{\text{charge}}[\theta^0] &= \frac{\hbar v}{\pi} \int dx \left(\frac{1}{2v^2} (\partial_t \theta^0)^2 - \frac{K}{2} (\partial_x \theta^0)^2 - V_{\text{charge}}(\theta^0 + m k_{\text{ext}} x - 2\tilde{A} \sin k_{\text{ext}} x) \right) \\ &\approx \frac{\hbar v}{\pi} \int dx \left(\frac{1}{2v^2} (\partial_t \theta^0)^2 - \frac{K}{2} (\partial_x \theta^0)^2 - g f_1^* \cos(4\theta^0 + m_{\text{tot}} k_{\text{ext}} x - 8\tilde{A} \sin k_{\text{ext}} x) \right), \end{aligned} \quad (125)$$

where the density (1) is related to the chemical potential μ by Eq. (50). The coupling constant g is given by its renormalized value (64) and the effective potential (63) is approximated in the last line of Eq. (125) utilizing Eq. (68).

It is crucial to note that in the strong coupling limit (74), the renormalized coupling $g \simeq 1/l_{\text{fl}}^2$ in the Lagrangian (125) does *not* depend on the density and on the external potential, as opposed to the weak coupling case of Section VII [e.g. Eqs. (97) and (121)]. Since this is a characteristic difference between the two limits that eventually yields to different excitation gap scaling, it is important to understand the physics behind it.

In the weak coupling limit the flavor soliton size l_{fl} depended on the external potential since the quantum fluctuations of the flavor sector were important on the scale of the potential period $\lambda_{\text{ext}} < l_{\text{fl}}$. Since the correla-

tion length l_{fl} of the neutral sector was greater than the potential period, the flavor fluctuations were sensitive to the shape of the external potential. Naturally, in that case the parameters of the potential could influence the renormalization group flow.

In the present case, $l_{\text{fl}} \ll \lambda_{\text{ext}}$, and the renormalization group produces the effective coupling g [Eq. (64)] on the scale $a < l < l_{\text{fl}}$ that appears “microscopic” for the external potential (11). In other words, the potential is adiabatic on the scale $l < l_{\text{fl}}$. However, a constant external potential has the same effect as the gate voltage. Although it can affect the local charge density, it does not affect the renormalization group flow. Thus both the flavor soliton scale l_{fl} and the renormalized coupling g in the strong coupling limit become independent on the details of the external potential.

B. Re-fermionization

The arguments that have led us to the charge mode Lagrangian (125) suggest an effective description of the strongly interacting nanotube electrons of four flavors in terms of a *single* mode. More precisely, we will assume below that one in fact can integrate out (eliminate) the neutral modes θ^α from the system (56) completely under the following conditions: (i) as long as we are interested in the charging properties of the system on the energy scale $\Delta_{\text{ch}} \gg \Delta_{\text{fl}}$ and on the spatial scale $l \gg l_{\text{fl}}$ that are greater than those for the flavor sector; (ii) the flavor correlations (*i.e.* the effects of the fermionic exchange) are negligible.

The latter condition deserves a special attention. At very low energy scale (of the order of the exchange integral between the adjacent flavor soliton cores) the effects of the fermionic exchange can be important. However, in the limit (74) this energy scale can be made arbitrarily small. One can make a case²⁶ that the flavor correlations can be discarded completely when the temperature (assumed to be zero in this work) is very small but larger than this exchange scale. Moreover, as we have mentioned above in Sec. VI E, the scale l_{fl} has a meaning of the correlation radius for the neutral modes. As long as we are interested in the physics of the charge mode on the length scale $l \sim \lambda_{\text{ext}} \gg l_{\text{fl}}$, the exponentially small

correlations of the flavor sector can be neglected.

With all that in mind, let us derive the effective single mode Hamiltonian for the nanotube in the strong coupling regime. Consider the charge mode Lagrangian (125). To present this Lagrangian in the canonical form suitable for subsequent re-fermionization we make the following change of variables:

$$\Theta = 2\theta^0 = \sum_{\alpha=1}^4 \Theta_\alpha . \quad (126)$$

The field Θ is the displacement field for the total density,

$$\rho = \frac{1}{\pi} \partial_x \Theta . \quad (127)$$

To preserve correct commutation relations, the canonical momentum Π_Θ for the field (126) should be half of that for the field θ^0 ,

$$\Pi_\Theta = \frac{1}{2} \Pi_{\theta^0} = \frac{1}{4} \sum_{\alpha=1}^4 \Pi_\alpha \quad (128)$$

with Π_α defined in Eq. (40). Changing variables in the Lagrangian (125) according to (126) and (128) we obtain the effective Lagrangian for the single mode Θ ,

$$\mathcal{L}_{\text{eff}}[\Theta] = \frac{\hbar v'}{\pi} \int dx \left\{ \frac{1}{2v'^2} (\partial_t \Theta)^2 - \frac{K'}{2} (\partial_x \Theta)^2 - g \cos(2\Theta + m_{\text{tot}} k_{\text{ext}} x - 2\tilde{A}' \sin k_{\text{ext}} x) \right\} , \quad (129)$$

with rescaled parameters

$$v' \equiv 4v , \quad K' \equiv \frac{K}{16} , \quad \text{and} \quad \tilde{A}' \equiv \frac{A}{K' \hbar k_{\text{ext}} v'} = 4\tilde{A} . \quad (130)$$

The re-definition of the parameters described by Eq. (130) has the following meaning. The velocity quadrupling simply states that we count incoming fermions regardless of their (four) flavors. The rescaling of the charge stiffness looks at first a bit puzzling. However, with the same accuracy that allowed us to discard the flavor modes, in the limit of $K \gg 1$, one may write

$$K' \approx 1 + \frac{(K-1)}{16} \equiv 1 + \nu' V(q) , \quad \nu' = \frac{1}{\pi \hbar v'} , \quad (131)$$

that is a definition for the charge stiffness for the spinless Dirac fermions of velocity v' , with ν' being the corresponding density of states [cf. Eq. (46)]. Finally, the chemical potential and the external potential amplitude are not rescaled [cf. Eqs. (49) and (58)].

Re-fermionizing the Lagrangian (129) by introducing the Dirac spinors $\Psi = (2\pi a')^{-1/2} e^{i\Theta}$, we formally obtain the effective Hamiltonian

$$\mathcal{H}_{\text{eff}}[\Psi] = \int dx \Psi^+ \{ -i\hbar v' \sigma_3 \partial_x + \Delta' \sigma_1 + U(x) - \mu \} \Psi + \frac{1}{2} \sum_k \rho_k V(k) \rho_{-k} \quad (132)$$

for the fictitious spinless Dirac fermions, where the total

fermion number density (16) in the new variables

$$\rho(x) = \Psi^+ \Psi . \quad (133)$$

The effective gap Δ' in Eq. (132) is chosen in such a way that it corresponds to the renormalized coupling (64) entering the Lagrangian (129),

$$g \simeq \frac{\Delta'}{\hbar v' a'}, \quad a' \simeq l_{\text{fl}} \quad (134)$$

similarly to the definition (45). In Eq. (134) the new length scale cutoff a' is assumed since the present approach is valid only at the length scales $l > l_{\text{fl}}$ beyond the correlation length of the neutral sector.⁴⁵ Eq. (134) together with Eqs. (64) and (79) yields

$$\Delta' \simeq \frac{\hbar v'}{l_{\text{fl}}} \simeq D^{1/5} \Delta_0^{4/5}. \quad (135)$$

To summarize, we have shown that in the limit when the fermionic exchange is unimportant due to exponentially small overlap of the flavor solitons, the NT electron dynamics can be described by the effective Hamiltonian (132) of *spinless* Dirac electrons. These fictitious fermions of the density (16) interact with each other by the *same* Coulomb potential (17) as do the original nanotube electrons. We stress here that neither the Coulomb potential $V(q)$ nor the external fields (external potential $U(x)$ and the chemical potential μ) are renormalized. That means that the fermions Ψ possess the same electron charge as the original nanotube electrons, which serves as a consistency check for the approach leading to the Hamiltonian (132).

C. Excitation gaps

The (charge) excitation gaps can be now estimated from the effective Lagrangian (129) or from the Hamiltonian (132). In the present subsection we will consider the case of a delocalized charge excitation

$$l_{\text{ch}} > \lambda_{\text{ext}} \quad (136)$$

that is spread over several potential minima. In this case one can apply the standard phase soliton approach for the single mode.³²

In the simplest case of integer *total* density m_{tot} one averages the potential term in the Lagrangian (129) over the potential period obtaining the effective coupling

$$g^{\text{strong}} = g J_{m_{\text{tot}}}(2\tilde{A}'), \quad (137)$$

performs integration over the quantum fluctuations of the Θ -field

$$g^{\text{strong}}(l) = g^{\text{strong}}(a') \left(\frac{l}{a'} \right)^{-\eta'}, \quad \eta' = \frac{1}{\sqrt{K'}} \simeq 4\eta, \quad (138)$$

with K' given by Eq. (131) and η by Eq. (83), finds the corresponding charge soliton scale self-consistently as

$$g^{\text{strong}}(l_{\text{ch}}) \simeq \frac{K'}{l_{\text{ch}}^2}, \quad (139)$$

and obtains the excitation gap

$$\Delta_m^{\text{strong}} \simeq \left| J_{m_{\text{tot}}}(2\tilde{A}') \right|^{\frac{1}{2-\eta'}} \Delta^{\text{strong}}, \quad m_{\text{tot}} = 0, \pm 1, \pm 2, \dots \quad (140)$$

Here the charge gap

$$\Delta^{\text{strong}} \simeq K^{\frac{1-\eta'}{2-\eta'}} \Delta' \quad (141)$$

with Δ' given by Eq. (135), and $J_{m_{\text{tot}}} \equiv J_{4m}$ being the Bessel function that depends on the *total* density (1).

When the total density $m_{\text{tot}} = p'/q'$ is a simple fraction, the charge density in the commensurate configuration is in general $q' \lambda_{\text{ext}}$ -periodic. To derive the effective Hamiltonian for the charged phase mode, one needs to perform the Pokrovsky–Talapov analysis³² for a single charge mode described by the Hamiltonian (129). For that, one performs the expansion

$$\Theta(x) = \bar{\Theta} + \Theta^{(1)} + \dots, \quad \Theta^{(n)} = \mathcal{O}(g^n) \quad (142)$$

in the (small) *renormalized* coupling (64), solves the corresponding Euler–Lagrange equations, and finds the effective potential for the “slow” phase mode $\bar{\Theta}$. The Hamiltonian for the charge mode will be of the form (4) with the potential energy $\sim g^{q'}$. The corresponding excitation gap can be estimated as energy of the phase soliton $\bar{\Theta}(x)$ (with quantum fluctuations of the $\bar{\Theta}$ field taken into account if necessary).

D. Classical limit

The effective Hamiltonian (132) admits a transparent classical limit. When the kinetic energy is negligible compared to the interaction, one may discard the zero-point motion of fermions and treat them as classical point electrons (with positions x_i) and holes (y_j) that interact with each other via the Coulomb potential. (One should remember that this “point charge” approximation is really valid on the length scale $l \gg l_{\text{fl}}$.) In this case one considers the classical energy of the system (132),

$$E_{\text{cl}} = \sum_{i=1..N_e} (\Delta' + U(x_i)) + \sum_{j=1..N_h} (\Delta' - U(y_j)) + \sum_{\substack{i,j=1 \\ i>j}}^{N_e} \frac{e^2}{|x_i - x_j|} + \sum_{\substack{i,j=1 \\ i>j}}^{N_h} \frac{e^2}{|y_i - y_j|} - \sum_{\substack{i,j=1 \\ i>j}}^{N_e, N_h} \frac{e^2}{|x_i - y_j|}. \quad (143)$$

Here N_e and N_h are the total number of electrons and holes in correspondingly minima and maxima of the external potentials (cf. Section II and Fig. 1). One can further introduce the cut-off for the long range Coulomb interactions by introducing the screening length l_s in the case when $l_s < L$, where L is the tube length. As in Section V, screening by the underlying substrate with the dielectric constant ϵ is trivially accounted for by substituting $e^2 \rightarrow 2e^2/(\epsilon + 1)$.

It is instructive to follow the connection between the classical limit (143) of the effective Hamiltonian (132) and the original charge mode Lagrangian (125) or (129). For that, let us represent the coordinates of the classical electrons in the state with the total density (1) by

$$x_j = x_j^{(0)} + \phi_j , \quad (144)$$

where ϕ_j are the displacements from the ideal positions

$$x_j^{(0)} = \frac{j\lambda_{\text{ext}}}{m_{\text{tot}}} \quad (145)$$

in the absence of the external potential. [For simplicity, we are not considering the holes in the maxima of $U(x)$, which can be treated analogously.] In the continual limit $\phi_j \equiv \phi(x_j) \approx \phi(x)$ the charge density is

$$\rho(x_j) \approx \frac{m_{\text{tot}} \partial_x \phi}{\lambda_{\text{ext}}} , \quad (146)$$

describing the change of ϕ by $\lambda_{\text{ext}}/m_{\text{tot}}$ when one extra particle is added. The third sum in Eq. (143) gives the interaction energy between the electrons. Substituting the coordinates (144) into this sum and expanding it up to the second order in $\phi_i - \phi_j \approx (x_i^{(0)} - x_j^{(0)}) \partial_x \phi$, we obtain the gradient term for the displacement mode energy,

$$\frac{1}{2} \int dx \left(2e^2 \ln \tilde{N} \right) \rho^2(x) \equiv \frac{\hbar v'}{\pi} \int dx \frac{\tilde{K}' (\partial_x \Theta)^2}{2} , \quad (147)$$

where

$$\Theta = \frac{\pi m_{\text{tot}}}{\lambda_{\text{ext}}} \phi(x) \quad (148)$$

is the net charge mode (126) defined in accord with the expression (127) for the total charge density, and the charge stiffness

$$\tilde{K}' = \frac{1}{\pi \hbar v'} \cdot 2e^2 \ln \tilde{N} \simeq K' - 1 \approx K' . \quad (149)$$

Here the stiffness K' is defined in Eq. (131), and the argument \tilde{N} of the Coulomb logarithm is found self-consistently as a number of electrons that belong to the soliton that describes the charge excitation. The expression (147) is the classical limit of the second term of the Lagrangian (129) with a meaning of the Coulomb interaction between the quasi-classical electrons. The non-linear term of the Lagrangian (129) gives the energy cost $\Delta' \cos(m_{\text{tot}} k_{\text{ext}} \delta\phi(x)) = \Delta'$ of adding one extra particle above the gap, $\delta\phi = \lambda_{\text{ext}}/m_{\text{tot}}$ according to Eq. (146). This term corresponds to the first term the classical energy (143). The interaction with the external potential $U(x)$ can be written in the usual form (20) and added to the argument of the cosine via the gauge transformation (53).

E. Discussion

The main result of this Section is the single-mode effective Hamiltonian (132) that allowed us to map the problem of the interacting fermions with the four flavors onto that of a single flavor and to utilize the standard phase soliton approach for the single mode.

What is the physical meaning of the approach that has lead to the effective Hamiltonian (132)? The crucial part of the derivation was finding the saddle point for the bosonic action (56) that depended on the strong electron-electron interactions. In the noninteracting case, fermions of the same flavor avoid each other due to the Pauli principle. The ground state wave function is then given by a product of the four Slater determinants, one for each flavor. However, when the repulsion between the fermions is strong, fermions of *all* the flavors avoid each other in a similar way, and the ground state wave function is a Slater determinant of a four-fold size. This is manifest in the $m_{\text{tot}} = 4m$ -dependence of the excitation gaps (140).

The original SU(4) flavor symmetry of the problem becomes manifest at the level of renormalization, namely in the particular scaling law of 4/5 of the renormalized gap (135) 'produced' via the renormalization group flow of the flavor sector at the length scales $a < l < l_{\text{fl}}$.

Let us discuss the results (140) and (141) in more detail. In the classical limit the charge excitation gap (141) for the stand-alone nanotube has the same form as that obtained in Sec. VI E above, Eq. (82):

$$\Delta^{\text{strong}} = \Delta \quad \text{when} \quad K \rightarrow \infty . \quad (150)$$

However, one notes that the power law exponents in the expressions (141) and (140) are *different* from those in Eqs. (84) and (99). This is not surprising since the theory (125) is different from the original model (56). Whereas in the latter the exchange is important, in the former the flavor sector is completely decoupled under the conditions specified above in Sec. VIII B. A similar situation has been observed in the recent calculation²⁶ for the spin-1/2 case and qualitatively explained in Ref. 46.

The question of charge-flavor (or charge-spin) decoupling deserves a special attention^{26,40,46} that goes beyond the scope of the present work. We would like to argue here that adding the external periodic potential can distinguish between spin-correlated and spin-decoupled regimes independently of the conditions set in Refs. 26 and 46. Indeed, the external potential (11) adds an extra length scale λ_{ext} that naturally distinguishes the regimes $l_{\text{fl}} > \lambda_{\text{ext}}$ and $l_{\text{fl}} < \lambda_{\text{ext}}$ dubbed here "weak" and "strong". Accordingly, the dependence on the *parameters of the potential* in these two regimes is crucially different, as one may see by comparing e.g. Eqs. (99) and (140) *even in the limit* $K \rightarrow \infty$.

Finally, in the present Section we have shown that the energy (143) is indeed a classical limit of the strong coupling Hamiltonian (132) and, therefore, the classical limit

of the whole problem (56) of strongly interacting nanotube electrons in the external fields. It is not surprising that the strong coupling limit of the problem is adiabatically connected to the classical limit; that is what is expected from the saddle-point approximation, with the quantum corrections around this saddle point yielding the renormalized Dirac gap Δ' . What is remarkable is that thanks to the Dirac nature of the nanotube spectrum and to the massive Thirring – sine–Gordon correspondence, the bosonization utilized in the present work is essentially exact and therefore allowed us to go all the way to the classical limit of the strongly interacting problem utilizing the saddle point treatment of the bosonic action of the four modes.

IX. PHASE DIAGRAM

In the present Section we will utilize the effective Hamiltonian (132) and its classical limit (143) to draw the phase diagram in the A, μ plane, Fig. 7, where A is the potential amplitude in Eq. (11). In this diagram, each region in Fig. 7 corresponds to a particular commensurate phase with the filling of $n_e = N_e/N$ electrons and $n_h = N_h/N$ holes per potential period, with $N = L/\lambda_{\text{ext}}$ [L is the tube length]. Such regions are labeled by pairs (n_e, n_h) as described in Section II, with the total density

$$m_{\text{tot}} = 4m = n_e - n_h \quad (151)$$

corresponding to Eq. (1). The underlying Dirac symmetry makes the phase diagram symmetric with respect to $\mu \leftrightarrow -\mu$, $n_e \leftrightarrow n_h$, so that only the $\mu > 0$ part is shown.

For simplicity, in this Section we will mainly consider the classical limit (143) and focus on the case of extremely delocalized charged excitation,

$$l_{\text{ch}} \sim l_s > L . \quad (152)$$

The nanotube in this case can be viewed as a sequence of quantum dots and anti-dots that are induced by the minima and maxima of the external potential. These dots are equivalent and in this respect the system becomes translationary invariant if one neglects effects of the finite system size L . Hence in the limit (152), by raising the chemical potential one adds an electron (hole) to *every* potential minimum (maximum), which results in adding $\sim N = L/\lambda_{\text{ext}} \gg 1$ particles to the tube of the length L . This simple observation leads to the following important consequences. First, *all* of the charge states characterized by the *total* density m_{tot} [m_{tot} either integer or fractional] are incompressible. Second, excitation gaps as a function of the potential amplitude A *never vanish* due to the charging energy $\sim \ln N$ of the Coulomb repulsion between the particles added into the different minima or maxima of $U(x)$.

The phase diagram in the classical limit consists of the regions that correspond to different incompressible

states, Fig. 7. It can be obtained by minimizing the energy functional

$$E_{\text{cl}} - \mu(N_e - N_h) \quad (153)$$

with respect to positions x_i and y_i of electrons and holes in the following way. We neglect the finite system effects and utilize translational invariance. In this case the optimal positions of electrons and holes relative to each potential minimum (maximum) are the same. To find them we minimize the functional

$$E_{n_e, n_h}(A) - \mu(n_e - n_h) \quad (154)$$

[which is the functional Eq. (153) per potential period], where the corresponding potential energy values calculated per λ_{ext} are

$$E_{10} = \Delta' - A + \frac{e^2}{\lambda_{\text{ext}}} \sum_{n=1}^{N/2} \frac{1}{n} , \quad (155)$$

$$E_{11} = 2E_{10} - \frac{2e^2}{\lambda_{\text{ext}}} \sum_{n=1}^{N/2} \frac{1}{n - \frac{1}{2}} , \quad (156)$$

$$E_{20} = \min_{\delta x} \left\{ 2\Delta' - 2A \cos k_{\text{ext}} \delta x + \frac{e^2}{2\delta x} + \frac{e^2}{\lambda_{\text{ext}}} \sum_{n=1}^{N/2} \left(\frac{2}{n} + \frac{1}{n + \frac{2\delta x}{\lambda_{\text{ext}}}} + \frac{1}{n - \frac{2\delta x}{\lambda_{\text{ext}}}} \right) \right\} \quad (157)$$

and so forth. While minimizing the energy E_{n_e, n_h} with respect to the positions of electrons and holes within each potential period, unphysical configurations of electrons on top of the holes are excluded by demanding that their minimum separation be e^2/Δ' . The latter condition takes into account the maximum exciton binding energy in the Dirac system.

Each border separating regions with different (n_e, n_h) is itself comprised of incompressible states with higher fractions m , as shown by the domain $(1/2, 0)$ between $(0, 0)$ and $(1, 0)$, reminiscent of the “devil’s staircase” behavior²⁸. The state $(1/2, 0)$ is characterized by a fractional total filling $m_{\text{tot}} = 1/2$ and has an electron in every other potential minimum.

As mentioned above, in the limit (152) the charge excitation is localized in every potential minimum. In this case one can further simplify the functional $E_{n_e, n_h}(A)$ by minimizing the interaction energy between the charges only in the same potential minimum (or maximum), treating the rest of the system in a mean-field way. In this case

$$E_{n_e, n_h} = (n_e + n_h)(\Delta' - A) + \frac{(n_e - n_h)^2 e^2}{2C_0} + V_{n_e} + V_{n_h} . \quad (158)$$

The first term in (158) is an energy of n_e electrons placed into each minimum and n_h holes into each maximum of $U(x)$. It corresponds to the first two terms of (143).

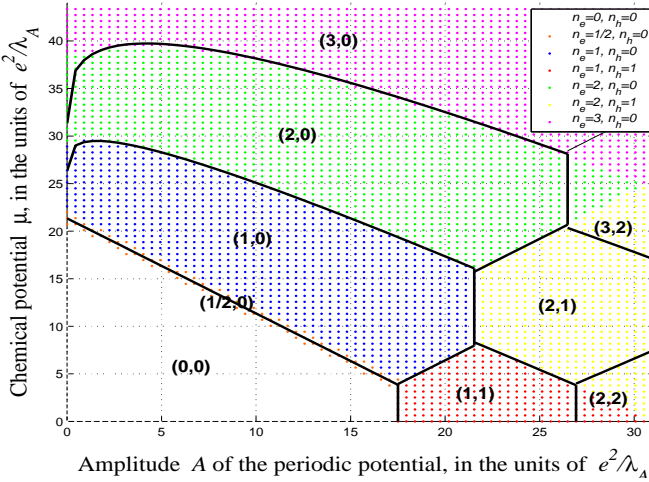


FIG. 7: Phase diagram for the nanotube, $\Delta' = 6\pi e^2/\lambda_{\text{ext}}$, $\ln(L/\lambda_{\text{ext}}) = 2.5$, $e^2/\lambda_{\text{ext}} = 1.44$ meV for $\lambda_{\text{ext}} = 1\mu\text{m}$. Color regions are the result of numerical minimization, black lines are approximations obtained from Eq. (158) with V_n given by Eq. (165).

The second term in (158) is the interaction energy of positive and negative charges located in the extrema of $U(x)$. Here

$$C_0 = \frac{\lambda_{\text{ext}}}{2\ln(L/\lambda_{\text{ext}})} \quad (159)$$

is a capacitance corresponding to the length λ_{ext} of a nanotube. If the screening length is smaller than system size, $l_s < L$, then L should be substituted by l_s in Eq. (159). Finally, V_n in (158) is the interaction energy of n electrons (or n holes) minimized with respect to their positions inside the corresponding potential well of the periodic potential (11). The Dirac symmetry yields $E_{n_e, n_h} = E_{n_h, n_e}$.

Let us study the charge filling diagram in more detail. For simplicity, we confine ourselves to the case of *integer* n_e and n_h . Due to the Dirac symmetry, it is enough to consider the case $\mu > 0$ corresponding to $n_e \geq n_h$. Minimization of Eq. (153) using the approximation (158) yields the filling diagram drafted in Fig. 8. Energy gaps corresponding to the incompressible states with the total density $n = n_e - n_h = (n_e + 1) - (n_h + 1) = \dots = (n_e + s) - (n_h + s)$ oscillate but do not vanish. Their minimum value

$$\delta\mu_{n_e, n_h}^{\min} = \frac{e^2}{C_0} \quad (160)$$

is determined solely by the NT charging energy and is independent of the details of interactions V_{n_e, n_h} inside each potential minimum. The regions (n_e, n_h) and $(n_e + 1, n_h + 1)$ of the filling diagram are separated by the vertical lines of fixed A , with its value implicitly defined by

$$A = \Delta' + \frac{1}{2} (V_{n_e+1}(A) - V_{n_e}(A) + V_{n_h+1}(A) - V_{n_h}(A)) . \quad (161)$$

Away from the values (161) the gap increases $\propto A$.

The model (158) can be treated exactly in the limiting cases of a few and of a large number of particles per each potential minimum. The former case relates to the filling diagram of Fig. 7 at $e^2/\lambda_{\text{ext}} < A \lesssim \Delta'$. The latter one is interesting since the corresponding excitation gaps cross over with those obtained in Section VIII [Eq. (140)]. In this case the charge filling diagram for the large A becomes universal (Fig. 8). Below we consider both cases.

A. Small fillings $n_e, n_h \sim 1$

The results of the numerical energy minimization (color in Fig. 7) can be fairly accurately reproduced (solid lines) by applying the approximation (158) for the case of a few particles per potential minimum (maximum). Below we will calculate the corresponding energies V_n , Eqs. (165).

When the Coulomb interaction is small,

$$\frac{e^2}{\lambda_{\text{ext}}} \ll A \lesssim \Delta' , \quad (162)$$

one can estimate the energies $V_{n_e, n_h}(A)$ by approximating each potential well of (11) by a quadratic polynomial:

$$U(x) \approx -A + \min_{n \leq N} \frac{M\Omega^2}{2} (x - (n + \frac{1}{2})\lambda_{\text{ext}})^2 . \quad (163)$$

Here M is a Dirac mass introduced in Eq. (31), and

$$\Omega^2 = \frac{Ak_{\text{ext}}^2}{M} . \quad (164)$$

Minimizing the Coulomb energy of n charges in a parabolic potential (163), we obtain first several values of V_n :

$$\begin{aligned} V_0 &= V_1 = 0 , \\ V_2 &= 3(\pi/2)^{2/3} \left(\frac{e^2}{\lambda_{\text{ext}}} \right)^{2/3} A^{1/3} , . \\ V_3 &= 5^{2/3} V_2(A) , \dots \end{aligned} \quad (165)$$

The power law correction $\sim A^{1/3}$ due to the above expressions is observed in Fig. 7 for $A \sim \Delta'$ as a deviation from the straight lines that separate different regions of the filling diagram.

For the yet smaller values of the potential amplitude $A \ll e^2/\lambda_{\text{ext}}$, the above perturbative treatment of interaction breaks down (solid lines in Fig. 7 deviate from the borders between the filling diagram regions obtained from the numerics). In this case it can be shown that the perturbation theory in A yields a regular behavior of the gap widths in accord with the numerical result shown in Fig. 7.

B. Large fillings $n_e, n_h \gg 1$

At large $n_e, n_h \gg 1$ the model (158) can be simplified by using the continuous description for the density of the

classical electrons (holes) inside each potential minimum (maximum). In this case, utilizing the Thomas–Fermi approximation, the charge density $\rho(x)$ in each minimum can be represented by the continuous function

$$\rho(x) \approx \rho_{\text{TF}} = -\frac{\pi n_e}{\lambda_{\text{ext}}} \cos k_{\text{ext}} x \quad (166)$$

that mimics the external potential profile (11). The density (166) is normalized to $n_e = \int_{\lambda_{\text{ext}}/4}^{3\lambda_{\text{ext}}/4} \rho_{\text{TF}}(x) dx$. The interaction energy V_{n_e} or V_{n_h} inside each “quantum dot” can be estimated as

$$V_{n_e} \simeq \frac{e^2}{2} \int_{\lambda_{\text{ext}}/4}^{3\lambda_{\text{ext}}/4} dx dx' \frac{\rho_{\text{TF}}(x)\rho_{\text{TF}}(x')}{|x-x'|} \equiv \frac{n_e^2 e^2}{2C_1}, \quad (167)$$

where the “dot capacitance”

$$C_1 = \frac{\lambda_{\text{ext}}}{2\pi \ln \frac{\lambda_{\text{ext}}}{a'}} \quad (168)$$

is independent of the potential amplitude A . The singularity in the integral in Eq. (167) is cut off on the scale $a' \sim l_{\text{fl}}$ of the order of the flavor soliton size, below which the quasiclassical description breaks down. The A -dependence of C_1 would appear as a correction to V_{n_e} with A -dependent integration limits in Eq. (167). The case V_{n_h} of the holes in the potential maxima (“anti-dots”) is analogous. Eq. (161) then yields the potential amplitude values that separate the configurations (n_e, n_h) and $(n_e + 1, n_h + 1)$:

$$A_{(n_e, n_h) \rightarrow (n_e + 1, n_h + 1)} = \Delta' + \frac{e^2}{2C_1} (n_e + n_h + 1). \quad (169)$$

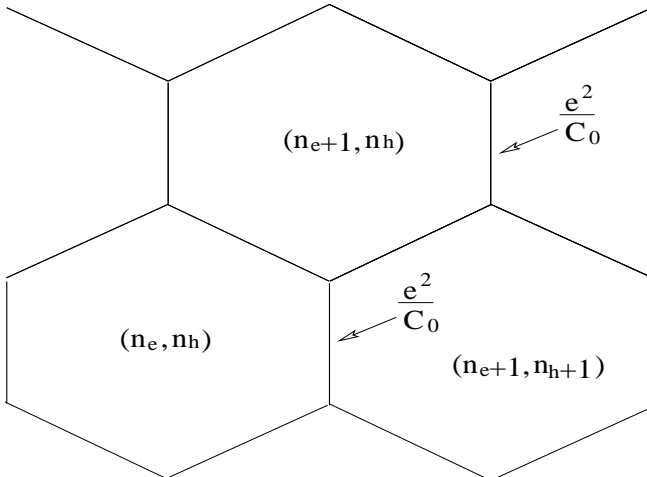


FIG. 8: Phase diagram in the (A, μ) plane according to the model (158). The minimum width of the gap for the incompressible state with any density $n_e - n_h$ is given by the NT charging energy (160). In the limit $n_e, n_h \gg 1$ all the regions of the filling diagram are identical, with their period in A given by Eq. (170).

In this limit all the “honeycomb” regions of the filling diagram in Fig. 8 are identical with their period in A being

$$\delta A_{n_e, n_h} = \frac{e^2}{C_1}. \quad (170)$$

Qualitatively, the honeycomb structure of Fig. 8 appears already for the moderate amplitudes A , as it can be seen in Fig. 7. The borders between the regions of the phase diagram in the limit $A > e^2/\lambda_{\text{ext}}, \Delta'$, are approximately linear, dominated by the linear dependence of E_{n_e, n_h} on A that stems from the first term of Eq. (158).

C. Crossover with the quantum case

Let us now show that the asymptotic values of the positions (169) of the gap minima derived in the previous subsection coincide with those derived in Section VIII utilizing the phase soliton approach. For that we assume that electrons in the subsequent potential minima and maxima do not interact with each other, that amounts to neglecting the second term $\sim e^2/C_0$ of the total energy (158). In this case the Thomas–Fermi approximation utilized above is equivalent to having the charged excitation screened in each potential minimum or maximum, with the screening length $l_s \approx \lambda_{\text{ext}}$.

Now recall that the excitation gaps (140) were oscillating as a function of the screened potential amplitude

$$\tilde{A}' = 4\tilde{A} = \frac{4A}{K\epsilon_0} \approx \frac{\pi}{2} \cdot \frac{A}{e^2/C_1}, \quad (171)$$

where we took the value of the charge stiffness (46) at the momentum scale $\lambda_{\text{ext}}^{-1}$ and substituted $K \rightarrow K - 1$ at $K \gg 1$. Utilizing the asymptotic behavior of the s -th zero of the Bessel function J_n ,

$$2\tilde{A}'_n^{(s)} \simeq \text{const} + \frac{\pi n}{2} + \pi s \quad (172)$$

[cf. Eqs. (140), (99), and (30)], we obtain the values of $A \simeq (n_e + n_h)e^2/2C_1$ in accord with Eq. (169). Here we made the obvious identifications $n \equiv m_{\text{tot}} = n_e - n_h$ and $s = \min\{n_e, n_h\}$. Away from these critical values the gap increases linearly in A similarly to what was stated above [after Eqs. (161) and (170)].

D. Discussion

In the present Section we utilized the classical limit (143) of the effective nanotube Hamiltonian (132) derived in the case when electrostatics of the charged mode is more important than the quantum effects like the zero point motion or the fermionic exchange. We have outlined the phase diagram whose limits are represented in Figs. 7 and 8. The phase diagram consists of the domains corresponding to the incompressible states with n_e electrons

and n_h holes with the total density (151). Only the most pronounced states are shown in Figs. 7 and 8. Their boundaries consist of the states with fractional densities $m_{\text{tot}} = p/q$ and the corresponding energy gaps rapidly decay with increasing the fraction denominator q , with the diagram having the structure of the devil's staircase. All of the states in Figs. 7 and 8 are incompressible in the classical limit.

We have found that energy gaps oscillate as a function of the potential amplitude A , as shown in Figs. 7 and 8. Such oscillations are similar to the ones observed in the quantum-mechanical cases for both the noninteracting electrons (Sec. IV and Fig. 2) and the weakly coupled interacting electrons (Sec. VII) described above.

X. QUANTIZED CURRENT

Let us discuss the experimental means of measuring the minigaps. For that we consider the setup suggested in the recent work, Ref. 24, in which the NT electrons in a periodic potential have been considered in connection with realizing the adiabatic charge pump of Thouless.²⁷ In the proposal,²⁴ the external periodic potential (11) originates from charge modulation in the underlying piezoelectric substrate due to the propagating surface acoustic wave (SAW). The potential amplitude A in Eq. (11) in this case can be as large as several hundred meV if the GaAs substrate is used as a piezoelectric,⁴⁷ and up to several eV in the case of a LiNbO₃ substrate. As mentioned in the Introduction to the present work, the adiabatically moving external potential can be also realized either optically or by time-varying periodic gating.

According to the classification of the present work, Ref. 24 dealt with the weak coupling limit for integer m fillings. For that case it has been shown, utilizing the theory of Thouless,²⁷ that when the chemical potential μ (calculated from the band center) is inside the m -th minigap Δ_m , adiabatically moving periodic potential induces the *quantized current*

$$j = m_{\text{tot}} e f, \quad m_{\text{tot}} = 4m, \quad m = \pm 1, \pm 2, \dots \quad (173)$$

in the nanotube. Here f is the frequency of the adiabatically changing periodic potential, four stands for the spin and valley degeneracy in a nanotube near half filling, and the negative values of m correspond to the hole part of the Dirac spectrum. The current (173) is an odd function of the chemical potential, reversing sign at half-filling and yielding no charge transport in the Dirac "vacuum" ($\mu = 0$). With typical SAW frequencies $f \sim 10$ GHz, adiabatic current (173) has been predicted to fall in the range of several nA.

Here we suggest that novel incompressible states with fractional m can be revealed in a setup of Ref. 24, with the adiabatic current (173) quantized in the corresponding *fractions* of $4ef$, where f is the frequency of the adiabatic periodic potential modulation. For that, the adi-

abaticity of transport should hold:

$$hf \ll \Delta_m, \quad (174)$$

where Δ_m is a (renormalized) minigap for the fractional m state. In the case of a moving SAW, this condition can be achieved since the substrate sound velocity is much smaller than the Fermi velocity in the nanotube. For $f = 10$ GHz corresponding to the SAW wavelength of the order of 1 μm , the energy $hf \approx 40$ μeV . Given typical minigap values Δ_m in the meV range, the adiabaticity condition (174) can be fulfilled. A similar SAW setup applied to pumping electrons between the two 2D electron gases through a pinched point contact⁴⁷ has a degree of adiabaticity that has a potential for becoming a standard of electric current.^{48,49} In the case when the moving potential is produced by adiabatic modulation of gate voltages on a periodic array of gates, there can be in principle even greater control of the sampling frequency f of the charge pumping, as well as of the amplitude and period of the potential.

Recently the SAW-assisted adiabatic pumping through the laterally defined quantum dot has been demonstrated.⁵⁰ The dot has been defined by metallic split gates in a GaAs/AlGaAs heterostructure. With the SAW period twice the size of the dot, the SAW-induced potential adiabatically modifies the local electrochemical potential that defines the dot, and carries an integer number of electrons each pumping cycle. Authors of Ref. 50 made an analogy of this setup with the Archimedean screw. Even more direct analog of the latter could be then realized by using the nanotube setup proposed in Ref. 24 for the case of the *fractional* filling m considered in the present work. Pumping in such a device would in this case critically depend on the electron interactions.

We emphasize here that the quantized current (173) being a topological invariant, is essentially a non-perturbative result.²⁷ To obtain Eq. (173) for the fractional- m case one needs to calculate the corresponding Chern class for the fully interacting system. This task is beyond the scope of the present work. However, a much simpler argument can be employed to justify Eq. (173) for the fractional m case.⁵¹

First let us note that both in Ref. 24 and in the present work, the external potential (11) has been treated non-perturbatively, which allowed to obtain the minigaps for the incompressible charge states in the closed form. In the classical limit of this problem considered in Section IX, the incompressible fractional- m states correspond to periodic configurations in which the classical electrons (holes) occupy the potential minima (maxima). With the chemical potential inside a corresponding minigap, the adiabatically moving external potential would drag charge carriers in a conveyor-belt fashion producing the current (173). The key argument is that in this limit the expression (173) is trivial, giving an average pumped charge per cycle in a *classical system*. As it is shown above, the classical limit of Section IX is adiabat-

ically continuable to the full quantum-mechanical problem. Utilizing the topological invariant property²⁷ of the result (173) concludes the proof of the current quantization in the generic quantum-mechanical case of the interacting electrons.

In a recent paper⁵² the case of pumping in an interacting quantum wire by a small time-varying external potential has been addressed. The perturbative treatment in the potential amplitude yields the non-quantized dc current whose frequency and temperature dependence is affected by electron interactions.⁵² Such a non-quantized current is analogous to that obtained from the Golden Rule in the noninteracting case.⁵³ However, the perturbative result was mis-interpreted by the authors of Ref.⁵² as a proof that the current is not quantized in the case when the density corresponds to a fractional number of electrons per potential period.

In conclusion, let us underscore that the proposed pumping measurement not only would realize the long-standing idea of the Thouless pump, but also would make the first example of the charge pump operating at the *fraction of the sampling frequency*, pumping on average a fractional number of electrons per period. The sole existence of the quantized current for the fractional m is due to the presence of electron-electron interactions. This setup would allow one to study the nature of the interactions in nanotubes in a greater detail, with having a variety of controllable experimental parameters at hand, such as the shape and frequency of the external potential, nanotube Dirac gap Δ_0 and the gate voltage, to name a few. By exploring the phase diagram for the system one can study effects of Wigner crystallization, quantum commensurate-incommensurate transitions, and the Tomonaga-Luttinger correlations.

Finally we note that the described setup can be utilized to adiabatically transport the low-energy strongly correlated SU(4) flavor states (*e.g.* those obeying the effective Gross-Neveu Lagrangian (100) described in Sec. VII) over a macroscopic distance, since the coupling to the adiabatically moving external potential is SU(4) invariant and thus it does not destroy spin or flavor correlations. We conjecture that such a setup hence may become useful for possible solid state implementations of quantum computers. Adding the external magnetic field would break the SU(4) symmetry down to SU(2) and has a potential to realizing the adiabatic quantized spin-polarized pump.

XI. CONCLUSIONS

In the present work we have shown that coupling of the interacting nanotube electrons to an external periodic potential is a very rich setup that allows one to study a number of effects of strongly correlated one-dimensional fermions.

The Dirac nature of the nanotube spectrum near half-filling allowed us to treat the problem of massive strongly interacting fermions of the four flavors essentially ex-

actly. In particular, we have been able to study how increasing the electron-electron interactions and the curvature of the electronic dispersion (controlled by the Dirac gap) drives the system from the Luttinger liquid of four modes into the Wigner crystal. While in the former limit the excitation gaps arise due to the Bragg diffraction of the delocalized quasiparticles of the four flavors, the latter limit maps onto the problem of the semi-classical commensurate-incommensurate transitions. Formally, this mapping has been achieved through the saddle-point treatment of the bosonized sine-Gordon action of the four modes. The saddle point in the limit of strong interactions has yielded the effective spinless Dirac Hamiltonian (132) for the nanotube in the Wigner crystal regime.

Let us briefly specify the main steps of our treatment. The NT electrons near half-filling were described [Section III] in the effective mass approximation as Dirac fermions of the four flavors. The Dirac symmetry of the half-filled NT Hamiltonian allowed us to utilize exact correspondence between the massive interacting Dirac fermions and the quantum sine-Gordon model. In particular, the Coulomb interaction between electrons was addressed non-perturbatively via the bosonization transformation (39). Finally, the external potential was also treated non-perturbatively by virtue of the gauge transformation (47). These steps allowed us to obtain the excitation gaps in the closed form [*e.g.* Eqs. (30), (99), (123) and (140)].

We have shown that the external periodic potential naturally distinguishes between the two physically different limits of the system, the Luttinger liquid of four modes, and the Wigner crystal. In both of these limits (called correspondingly “weak” and “strong”) we identified novel incompressible charge states characterized by a fractional number m of electrons of each flavor per potential period, corresponding to the density (1). Such fractional states exist only in the presence of the electron interactions.

Quantum fluctuations of the soft flavor sector are shown to strongly renormalize the couplings, providing the effective action for the stiff charge mode. For the weak coupling limit (2) the effective Hamiltonian has been derived in Section VII for the case of integer fillings, Eq. (96), and for the simplest case of a fractional filling $m = 1/2$, Eq. (122). For the case of the strong coupling (3), the corresponding renormalized Hamiltonian is given by Eq. (132).

To estimate the energy gaps for the incompressible states we utilized the phase soliton approach. This approach was generalized for the case of four quantum modes in the weak coupling limit in Section VII. We showed that minigaps in the interacting system generally oscillate as a function of the amplitude of the external potential. The value of these minigaps, as well as their power-law scaling due to the Tomonaga-Luttinger correlations, can serve as a probe of the strength of the electron-electron interactions in nanotubes. We also found that the effective flavor excitations are governed

by the Gross–Neveu Lagrangian of the form (100).

The strong coupling limit (3) was addressed in Section VIII. There we showed that the NT electrons of the four flavors behave similarly to the system of the Dirac fermions of a single flavor with the total density (1). As a result, the renormalized excitation gaps (140) in this case are the function of the total density $m_{\text{tot}} = 4m$. Physically, this happens because in the limit of a strong Coulomb repulsion, the fermions of the same and of the different flavors avoid each other in a similar fashion. The phase diagram for the system was sketched for the semi-classical limit of the problem in Section IX. It has a structure of a devil's staircase. In Figs. 7 and 8, different regions correspond to the different number (integer or fractional) of electrons and holes per potential period.

Finally, we proposed the setup of adiabatic charge pump to study the phase diagram experimentally. This setup allows one to detect the interaction-induced

incompressible electron states of nanotube electrons, study electron–electron interactions and transition to the Wigner crystal regime in greater detail, as well as to realize the quantized charge pump (“Archimedean screw”) that pumps a fraction of electron charge per cycle due to electron–electron interactions.

Acknowledgments

It is a pleasure to thank Leonid Levitov for bringing this problem to the author's attention, for fruitful discussions, as well as for the suggestions on the earlier versions of the manuscript. This work was initiated at MIT (supported by NSF MRSEC grant DMR 98-08941) and completed at Princeton (supported by NSF MRSEC grant DMR 02-13706).

* Electronic address: dima@alum.mit.edu

¹ S. Iijima, *Nature* **354**, 56–58 (1991)

² R. Saito, G. Dresselhaus and M. S. Dresselhaus, *Physical Properties of Carbon Nanotubes*, Imperial College Press, London, 1998.

³ M.S. Dresselhaus, G. Dresselhaus, Ph. Avouris, *Carbon Nanotubes: Synthesis, Structure, Properties and Applications*, Springer Verlag, New York, 2001

⁴ P.L. McEuen, *Nature* **393**, 15 (1998)

⁵ C. Dekker, *Physics Today*, May 1999, p. 22

⁶ P.M. Ajayan and O.Z. Zhou, in the book³

⁷ P. Avouris, *Acc. Chem. Res.* **35**, 1026 (2002)

⁸ D. Rotman, *Technology Review* **105**, 37 (March 2002)

⁹ Y.A. Krotov, D.-H. Lee, S.G. Louie, *Phys. Rev. Lett.* **78**, 4245 (1997)

¹⁰ R. Egger, A. O. Gogolin, *Phys. Rev. Lett.* **79**, 5082 (1997)

¹¹ C. Kane, L. Balents, M. P. A. Fisher, *Phys. Rev. Lett.* **79**, 5086 (1997)

¹² A. Odintsov and H. Yoshioka, *Phys. Rev. Lett.* **82**, 374 (1999)

¹³ L. S. Levitov, A. M. Tsvelik, *Phys. Rev. Lett.* **90**, 016401 (2003); [cond-mat/0205344](https://arxiv.org/abs/cond-mat/0205344)

¹⁴ M. Stone (Ed.), *Bosonization*, World Scientific, Singapore (1994)

¹⁵ M. Bockrath, D. H. Cobden, P. L. McEuen, N. G. Chopra, A. Zettl, A. Thess, R. E. Smalley, *Science* **275**, 1922 (1997)

¹⁶ S. Tans, M.H. Devoret, R. Groeneveld and C. Dekker, *Nature* **394**, 761 (1998)

¹⁷ M. Bockrath, D. H. Cobden, Jia Lu, A. G. Rinzler, R. E. Smalley, L. Balents, P. L. McEuen, *Nature* **397**, 598 (1999)

¹⁸ Z. Yao, H. W. Ch. Postma, L. Balents, C. Dekker, *Nature* **402**, 273 (1999)

¹⁹ J. Nygard, D.H. Cobden, M. Bockrath, P.L. McEuen, P.E. Lindelof, *Applied Physics A* **69**, 297 (1999)

²⁰ H. Ishii, H. Kataura, H. Shiozawa, H. Yoshioka, H. Otsubo, Y. Takayama, T. Miyahara, S. Suzuki, Y. Achiba, M. Nakatake, T. Narimura, M. Higashiguchi, K. Shimada, H. Namatame and M. Taniguchi, *Nature (London)* **426**, 540 (2003)

²¹ K.A. Matveev, *Phys. Rev. Lett.* **92**, 106801 (2004)

²² S. Coleman, *Phys. Rev. D* **11**, 2088 (1975)

²³ F.D.M. Haldane, *J. Phys. A* **15**, 507 (1982)

²⁴ V.I. Talyanskii, D.S. Novikov, B.D. Simons, L.S. Levitov, *Phys. Rev. Lett.* **87**, 276802 (2001); [cond-mat/0105220](https://arxiv.org/abs/cond-mat/0105220)

²⁵ M. Ogata and H. Shiba, *Phys. Rev. B* **41**, 2326 (1990)

²⁶ V.V. Cheianov and M.B. Zvonarev, preprint [cond-mat/0308470](https://arxiv.org/abs/cond-mat/0308470); *J. Phys. A* **37**, 2261 (2004)

²⁷ D. J. Thouless, *Phys. Rev. B* **27**, 6083 (1983)

²⁸ P. Bak, *Rep. Prog. Phys.* **45**, 587 (1982)

²⁹ J. Frenkel and T.A. Kontorova, *Zh. Eksp. Teor. Fiz.* **8**, 1340 (1938)

³⁰ F.C. Frank and J.H. van der Merwe, *Proc. Roy. Soc.* **198**, 205, 216 (1949)

³¹ I.E. Dzyaloshinsky, *Zh.E.T.F.* **47**, 1420 (1964);

³² V.L. Pokrovsky, A.L. Talapov, *Sov. Phys. JETP* **75**, 1151 (1978);

³³ D. P. DiVincenzo and E. J. Mele, *Phys. Rev. B* **29**, 1685 (1984)

³⁴ C. L. Kane and E. J. Mele, *Phys. Rev. Lett.* **78**, 1932 (1997)

³⁵ C. Zhou, J. Kong, and H. Dai, *Phys. Rev. Lett.* **84**, 5604 (2000); M. Ouyang, J.L. Huang, C.L. Cheung, C.M. Lieber, *Science* **292**, 5517 (2001)

³⁶ H. Ajiki and T. Ando, *J. Phys. Soc. Jpn.* **65**, 505 (1996).

³⁷ J. -O. Lee, J. R. Kim, J. J. Kim, J. Kim, N. Kim, J. W. Park, and K. H. Yoo, *Sol. Stat. Comm.* **115**, 467 (2000).

³⁸ To be precise, this statement is true in the forward scattering approximation that holds down to undetectably small energies where interaction-induced gaps may open.^{9–12}

³⁹ The author thanks A.M. Polyakov for a discussion on renormalization

⁴⁰ D.S. Novikov, unpublished

⁴¹ K. Wilson, *Phys. Rev.* **179**, 1499 (1969); C.G. Callan, *Phys. Rev. D* **2**, 1541 (1970); K. Symanzik, *Commun. Math. Phys.* **18**, 227 (1970)

⁴² Similar expression for renormalized gap Δ has been obtained earlier in Ref. 13. Whereas we agree on scaling exponents of D and Δ_0 , the K –dependence is different. The procedure of Ref. 13 yields the prefactor $K^{1/5}$ instead of the more natural result $K^{1/2+\mathcal{O}(\eta)}$ that matches the clas-

sical limit. We believe this discrepancy is a consequence of oversimplifying the renormalization group treatment by introducing a *single* soliton scale under the RG in Ref. 13.

⁴³ D.J. Gross and A. Neveu, Phys. Rev. D **10**, 3235 (1974)

⁴⁴ A.B. Zamolodchikov and Al.B. Zamolodchikov, Ann. Phys. **120**, 253 (1979)

⁴⁵ Here we also do not distinguish between $\ln(l_s/a)$ and $\ln(l_s/a')$ in the Coulomb formfactor $V(q)$, with large $K \gg 1$ implying large screening length $l_s \sim l_{\text{ch}} \gg a, a'$. This corresponds to treating the tube *capacitance* with logarithmic accuracy.

⁴⁶ G.A. Fiete and L. Balents, preprint [cond-mat/0403744](https://arxiv.org/abs/cond-mat/0403744)

⁴⁷ J.M. Shilton, V.I. Talyanskii, M. Pepper, D.A. Ritchie, J.E.F. Frost, C.J.B. Ford, C.G. Smith, G.A.C. Jones, J. Phys. Condens. Matter **8**, L531 (1996); V.I. Talyanskii, J.M. Shilton, M. Pepper, C.G. Smith, C.J.B. Ford, E.H. Linfield, D.A. Ritchie, G.A.C. Jones, Phys. Rev. B **56**, 15180 (1997).

⁴⁸ Q. Niu, Phys. Rev. Lett. **64**, 1812 (1990)

⁴⁹ J. Cunningham, V.I. Talyanskii, J.M. Shilton, M. Pepper, A. Kristensen, P.E. Lindelof, J. Low Temp. Phys. **118**, 555 (2000)

⁵⁰ J. Ebbecke, N.E. Fletcher, T.J.B.M. Janssen, F.J. Ahlers, M. Pepper, H.E. Beere, and D.A. Ritchie, Appl. Phys. Lett. **84**, 4319 (2004); preprint [cond-mat/0312304](https://arxiv.org/abs/cond-mat/0312304)

⁵¹ Q. Niu and D.J. Thouless, J. Phys. A **17**, 2453 (1984)

⁵² R. Citro, N. Andrei, and Q. Niu, Phys. Rev. B **68**, 165312 (2003)

⁵³ D.S. Novikov, Ph.D. Thesis, Massachusetts Institute of Technology (2003), unpublished